Suppression of the RAS/ERK pathway by Tmsb10 is the key step for promoting fetal Leydig cell differentiation from progenitors

Miki Inoue
Kyushu University https://orcid.org/0000-0003-3581-9852
Takashi Baba
Kyushu University
Fumiya Takahashi
Kyushu University
Miho Terao
National Research Institute for Child Health and Development
Shogo Yanai
Kyushu University
Yuichi Shima
Kyushu University
Daisuke Saito
Kyushu University
Kei Sugihara
Kyushu University
Takashi Miura
Kyushu University
Shuji Takada
National Research Institute for Child Health and Development
Mikita Suyama
Kyushu University https://orcid.org/0000-0001-9526-3193
Yasuyuki Ohkawa
Kyushu University https://orcid.org/0000-0001-6440-9954
Ken-ichirou Morohashi (morohashi.ken-ichirou.874@m.kyushu-u.ac.jp)
Kyushu University

Article

Keywords:

Posted Date: February 16th, 2022

DOI: https://doi.org/10.21203/rs.3.rs-1357916/v1

Version of Record: A version of this preprint was published at Communications Biology on September 15th, 2022. See the published version at https://doi.org/10.1038/s42003-022-03941-5.

Suppression of the RAS/ERK pathway by *Tmsb10* is the key step for promoting fetal Leydig cell differentiation from progenitors

Miki Inoue[1,2], Takashi Baba[1,2], Fumiya Takahashi[1], Miho Terao[3], Shogo Yanai[1], Yuichi Shima[1,2], Daisuke Saito[1,4], Kei Sugihara[5], Takashi Miura[5], Shuji Takada[3], Mikita Suyama[1,4], Yasuyuki Ohkawa[1,5], Ken-ichirou Morohashi[1,2]*

1, Department of Systems Life Sciences, Graduate School of Systems Life Sciences, Kyushu University, Maidashi 3-1-1, Higashi-ku, Fukuoka, 812-8582, Japan.

2, Department of Molecular Biology, Graduate School of Medical Sciences, Kyushu University, Maidashi 3-1-1, Higashi-ku, Fukuoka, 812-8582, Japan.

3, Department of Systems BioMedicine, National Research Institute for Child Health and Development, 2-10-1 Okura, Setagaya-ku, Tokyo 157-8535, Japan.

4, Division of Bioinformatics, Medical Institute of Bioregulation, Kyushu University, Maidashi 3-1-1, Higashi-ku, Fukuoka 812-8582, Japan.

5, Department of Anatomy and Cell Biology, Graduate School of Medical Sciences, Kyushu University, Maidashi 3-1-1, Higashi-ku, Fukuoka, 812-8582, Japan.

* To whom correspondence should be addressed.

20 Department of Molecular Biology, Graduate School of Medical Sciences, Kyushu University,

21 Maidashi 3-1-1, Higashi-ku, Fukuoka 812-8582, Japan

22 e-mail; morohashi.ken-ichirou.874@m.kyushu-u.ac.jp

23

24 ***Disclosure statement:*** The authors have nothing to disclose.

ABSTRACT

Leydig cells in fetal testes play crucial roles in masculinizing fetuses through androgen production. Gene knockout studies have revealed that growth factors are implicated in fetal Leydig cell (FLC) differentiation, but little is known about the mechanisms regulating this process. We investigated this issue by characterizing FLC progenitor cells using single-cell RNA sequencing. The sequence datasets suggested that *thymosin β10* (*Tmsb10*) was transiently upregulated in the progenitors. While studying the function of *Tmsb10*, we revealed that platelet-derived growth factor (PDGF) regulated ciliogenesis through the RAS/ERK and PI3K/AKT pathways, and thereby promoted desert hedgehog (DHH)-dependent FLC differentiation. *Tmsb10* expressed in the progenitor cells induced their differentiation into FLCs by suppressing the RAS/ERK pathway. Through characterizing the transiently expressed *Tmsb10* in the FLC progenitors, this study unveiled the molecular process of FLC differentiation and showed that it is cooperatively induced by DHH and PDGF.

INTRODUCTION

Two types of somatic cells, Sertoli and Leydig cells, play unique and mutually complementary roles to achieve testicular functions. Sertoli cells provide germ cells with nutrients and stimuli to support their differentiation, while Leydig cells produce a potent androgen, testosterone, that regulates the differentiation and functions of both germ and Sertoli cells[1]. In addition to these intratesticular functions, testosterone induces a variety of male traits throughout the body. Unlike other vertebrates, mammalian species possess two developmentally different Leydig cells, fetal-type Leydig cells (FLCs) and adult-type Leydig cells (ALCs), the former of which play pivotal roles in the masculinization of fetuses through androgen production[2].

Several studies using gene-disrupted mice have revealed the involvement of multiple growth factors and their receptors in gonad development. Among them, desert hedgehog (DHH), NOTCH, platelet-derived growth factor (PDGF), and transforming growth factor β (TGFβ) signals were implicated in FLC differentiation; disruption of these genes resulted in aberrant FLC differentiation[3-6]. Likewise, genes encoding transcription factors such as *aristaless related homeobox* (*Arx*)[7], *podocyte-expressed 1/transcription factor 21* (*Pod1/Tcf21*)[8], *adrenal 4-binding protein/ steroidogenic factor-1* (*Ad4BP/SF-1*, *Nr5a1*)[9,10], glioma-associated Krüppel-type Zn finger protein (*Gli1/Gli2*) [11], and *Gli3*[12] were found to contribute to FLC differentiation as demonstrated in gene knockout (KO) mice. Moreover, possible FLC progenitor cells have been shown to express ARX[13], MAFB[14], Notch[15,16], Nestin[17], and *Wnt5a*[18,19]. Therefore, several

58 studies have shown that multiple factors are involved in the differentiation of FLCs. However, it
59 remains unclear how these factors result in the formation of FLC progenitor cells and then
60 promote their successive differentiation into FLCs.

61 Studies concerning hedgehog (HH) signaling have unveiled the complex mechanism of
62 intracellular signal transduction. Upon binding of HH to its receptor Patched (PTCH),
63 Smoothened (SMO) is released from inhibition by the receptor and then accumulates in the
64 primary cilium[20]. Thereafter, SMO undergoes phosphorylation, and in this form it promotes
65 dissociation of GLI from kinesin family protein 7 and Suppressor of fused. Ultimately, GLI is
66 converted to an active form and then begins to transcribe HH target genes[21].

67 Studies of PDGF signaling have demonstrated that two receptors, PDGFRα and PDGFRβ,
68 transduce signals upon binding to four ligand molecules, PDGF-A, PDGF-B, PDGF-C, and
69 PDGF-D[22]. The ligand-bound receptors activate the RAS/ERK pathway by successive
70 phosphorylation of its components. It has also been shown that RAS activates the PI3K/AKT
71 pathway, in which phosphatidylinositol 3-phosphate (PIP_3), which is synthesized by PI3K, plays
72 a pivotal role in activating PDK1 and AKT. By regulating these signal pathways, PDGFs are
73 involved in a variety of cellular processes such as differentiation, proliferation, metabolism, and
74 migration[22]. As described above, the specific mechanisms of DHH and PDGF signal
75 transduction have been uncovered gradually. Unfortunately, however, it remains largely
76 unknown how these growth factors promote FLC differentiation.

77 Thymosins were originally isolated from the calf thymus[23]. Among them, TMSB4X
78 (thymosin beta 4, X chromosome) and TMSB10 (thymosin beta 10), which are members of the
79 β-thymosin family, have highly homologous amino acid sequences. The expression of these β-
80 thymosins has been observed in a variety of normal and cancer cells[24-26]. As for their functions,
81 TMSB4X was shown to sequester actin monomer to suppress the formation of filamentous
82 actin[27]. Likewise, TMSB10 suppresses actin polymerization through the actin-binding sequence
83 conserved in these β-thymosins[28]. Related to their actin-sequestering function, many studies
84 have reported that these β-thymosins are potentially involved in processes such as blood vessel
85 formation, wound healing, cell migration, and cancer metastasis[29]. Moreover, TMSB10, but not
86 TMSB4X, interacts directly with RAS to inhibit RAS-RAF interaction, which disturbs
87 downstream signal transduction[30].
88 In the present study, we examined the interstitial cells of developing fetal testes in mice
89 using single-cell RNA sequencing (scRNA-seq). Analyses of the sequence datasets found a
90 unique cell fraction potentially consisting of FLC progenitors. Among the genes whose
91 expression was upregulated in the progenitor cells, we focused on *Tmsb10*. We found that
92 PDGF regulated the formation of primary cilia via signaling in the RAS/ERK and PI3K/AKT
93 pathways, and moreover that TMSB10 promoted ciliation by hindering the interaction between
94 RAS and RAF, thereby suppressing the RAS/ERK signal pathway. This study unveils, for the
95 first time, part of the molecular process of FLC differentiation that is induced cooperatively by
96 DHH and PDGF.

RESULTS

FLC progenitor cells are present in the interstitial space of fetal testes

A transgenic *FLE-EGFP* mouse was established using the fetal Leydig-specific enhancer (FLE) and promoter region of *Ad4BP/SF-1* gene[31]. FLCs in the fetal testes of the transgenic mice were strongly labeled with EGFP (S-EGFP cells), and a large population of interstitial cells was labeled only weakly with EGFP (W-EGFP cells). Both S-EGFP and W-EGFP cells could be recovered separately by fluorescence-activated cell sorting (FACS) from E16.5 fetal testes[32]. Because FLCs at this stage increase in number even though they scarcely proliferate[13,17,33], we anticipated that the W-EGFP cell population may include FLC progenitor cells. Indeed, *in vitro* testis reconstruction studies demonstrated that some W-EGFP cells, if not all, have the potential to differentiate into FLCs[34].

To identify the FLC progenitors, 696 W-EGFP cells and 92 S-EGFP cells prepared from E16.5 fetal testes were subjected to scRNA-seq[35]. After low-quality scRNA-seq datasets were removed, 341 and 80 datasets obtained from the W-EGFP and S-EGFP cells, respectively, were subjected to subsequent analyses (Supplementary Table 1).

To assess how many cell types were present among the W-EGFP cells, the datasets were subjected to hierarchical clustering on the significant principal components. As indicated in the cluster dendrogram in Fig. 1a, the W-EGFP cells were divided into three clusters (clusters A, B, and C), while the S-EGFP cells were divided into two clusters (clusters D and E). According to the relative distances between the clusters, cluster E was the most distant from the other

clusters, while clusters A and B were not clearly segregated. Interestingly, clusters C and D, which were originally derived from the W-EGFP and S-EGFP cells, respectively, demonstrated an intimate correlation. A similar distribution of the five cell clusters was observed by t-distributed stochastic neighboring embedding (t-SNE) (Fig. 1b).

The scRNA-seq data were further subjected to Monocle trajectory analysis to predict the developmental trajectory of the five cell clusters. As indicated in Fig. 1c, the cells in clusters A and B were predicted to differentiate into those in cluster C, and eventually, via cluster D, into those in cluster E. Because the cells in cluster E are FLCs, as described later, characterization of the putative progenitor cells in cluster C seemed to be critical for uncovering the mechanism of FLC differentiation.

Therefore, a heatmap of gene expression was generated using the genes whose expression was altered in clusters C, D, and E (Fig. 1a). The genes in group I showed higher expression in cluster E and/or cluster D. FLC marker genes such as *insulin-like 3* (*Insl3*)[36,37], *cholesterol side-chain cleavage enzyme cytochrome 450* (*Cyp11a1*), and *3β-hydroxysteroid dehydrogenase* (*Hsd3b1*)[38-40] were included in this group, indicating that the cells in clusters D and E consisted of immature and mature FLCs, respectively. The genes in group II showed higher expression in clusters C, D, and E. Interestingly, several genes encoding large ribosomal subunits were included in this group. Finally, the genes in group III showed higher expression in cluster C.

Expression of* Tmsb10 *is transiently upregulated in putative FLC progenitors

Expression levels of the genes above were depicted colorimetrically on the cells whose distribution was determined by t-SNE (Fig. 1d-f, Supplemental Fig 1a). As expected, the highest expression of *Cyp11a1* was seen in cluster E, that of *calreticulin* (*Calr*) was in clusters C, D, and E, and that of *Tmsb10* was in cluster C. Considering that the cells in cluster C are FLC progenitors, the expression of *Tmsb10* appeared to be transiently upregulated during differentiation into FLCs. The expression pattern of *Tmsb4x*, another member of β-thymosin family, was different from that of *Tmsb10* (Supplementary Fig. 1b). We previously showed that the expression of ARX is gradually decreased in interstitial cells that are differentiating into FLCs[13]. Consistent with the previous observation, *Arx* expression appeared to be decreased in cluster C and then further decreased in clusters D and E (Fig. 1g).

TMSB10 is expressed in the interstitial cells of fetal testes

Focusing on the gene expression profile of the genes in group III, we investigated whether *Tmsb10* is involved in FLC differentiation. First, we attempted to identify the cells expressing TMSB10 in fetal testes. Because no available antibody recognized TMSB10, we generated knock-in mice in which *mCherry* was inserted at the *Tmsb10* locus (Supplementary Fig. 2). The mice were then crossed with *FLE-EGFP* mice, and then the fetal testes of the double transgenic mice at E16.5 were examined. TMSB10 (mCherry) did not seem to be expressed in FLCs (S-EGFP cells) (open arrowheads in Fig. 2a). Strong signals for TMSB10 were detected in the interstitial space, and they were colocalized with laminin (arrows). Considering that laminin is a

157 marker of endothelial cells (Supplementary Fig. 3), TMSB10 was thought to be strongly
158 expressed in the cells. Further, cells exhibiting weak TMSB10 signals were present in the
159 interstitial space (closed arrowheads), and some of these cells were weakly stained with EGFP.
160 To exclude the possibility that the W-EGFP cell population includes *Tmsb10*-expressing
161 endothelial cells, we examined the expression of the endothelial cell marker *Pecam1* in W-
162 EGFP, S-EGFP, and EGFP-negative cells. qRT-PCR revealed that *Pecam1*-positive endothelial
163 cells were mostly recovered in EGFP-negative cells but not in W-EGFP cells (Fig. 2b-d),
164 indicating that W-EGFP cells include TMSB10-positive cells other than endothelial cells.
165
166 **Tmsb10** ***is required for FLC differentiation***
167 As described previously[34], we established a testis reconstruction system using W-EGFP
168 cells mixed with whole cells prepared from wild-type fetal testes (Fig. 3a). Using this system,
169 we succeeded in recapitulating FLC differentiation from W-EGFP cells by detecting the
170 appearance of cells strongly positive for EGFP (equivalent to S-EGFP cells) (Fig. 3b). A
171 previous gene disruption study demonstrated that DHH is required for differentiation of FLCs[3].
172 Thus, we investigated whether DHH stimulates FLC differentiation using *in vitro* reconstructed
173 testes. As shown in Fig. 3c and d, EGFP signals in the reconstructed testes increased when
174 incubated in the presence of a SMO agonist (SAG).
175 Considering the transiently upregulated expression of *Tmsb10* in the putative progenitor
176 cells, we hypothesized that *Tmsb10* plays a critical role in FLC differentiation. Thus, we

177 examined whether *Tmsb10* knockdown (KD) impacted FLC differentiation in the reconstructed
178 testes. Cultured W-EGFP cells were treated with the siRNAs for *Tmsb10*, *Tmsb4x*, and
179 *Ad4BP/SF-1*. As expected, these treatments resulted in a clear reduction of the expression of
180 each corresponding gene (Supplementary Fig. 4). Then, we utilized these KD cells for *in vitro*
181 testis reconstruction assays. *Tmsb10* KD was found to impair the ability of W-EGFP cells to
182 differentiate into S-EGFP FLCs, although this impairment was not observed following
183 treatment with si*Tmsb4x* or control siRNA (si*Cnt*) (Fig. 3e). It has been established that
184 *Ad4BP/SF-1* is essential for steroidogenic cell differentiation[9,10,41,42]. As expected, FLC
185 differentiation was markedly affected by *Ad4BP/SF-1* KD (Fig. 3e). Quantitative examination
186 indicated that *Tmsb10* KD decreased the differentiation efficacy to 37% of control, whereas it
187 was unaffected by *Tmsb4x* KD (Fig. 3f). *Ad4BP/SF-1* KD resulted in a reduction of more than
188 90%. Similar effects of *Tmsb10* KD on FLC differentiation were observed in the presence of
189 SAG (Fig. 3g, h).
190 Finally, we examined whether activity downstream of HH signaling was affected by
191 *Tmsb10* KD. *Gli1* gene expression is known to be activated by HH signaling[21]. As expected,
192 *Tmsb10* KD resulted in a decrease of *Gli1* expression (Fig. 3i), while *Tmsb4x* KD had no effect
193 (Supplementary Fig. 5a-c). Taken together, these results strongly suggest that *Tmsb10* is
194 required for FLC differentiation through regulating HH signaling.
195
196 **Tmsb10** ***regulates primary cilia formation by inhibiting the RAS/ERK pathway***

Because the primary cilium is a unique structure that is essential for HH signal transduction[20], we examined whether *Tmsb10* was implicated in the regulation of ciliogenesis. Consistent with the observation that primary cilia emerge only during the G0/G1 cell cycle phase[43], we scarcely detected them in W-EGFP cells cultured in serum-containing medium. Therefore, W-EGFP cells were cultured in serum-free medium for 24 h before the following immunofluorescence studies were performed. Under this condition, approximately 70% of the W-EGFP cells were ciliated. Notably, the number of ciliated cells was dose-dependently decreased by si*Tmsb10* treatment (Fig. 4a, b), whereas si*Cnt* treatment had no effect. The number of ciliated cells was decreased to 45% relative to baseline by KD with si*Tmsb10* at a concentration of 10.0 nM. Treatments with higher concentrations resulted in decreased survival of W-EGFP cells. Therefore, the following *Tmsb10* KD experiments were performed using a concentration of 10.0 nM. A similar decrease in the number of ciliated cells was seen when W-EGFP cells cultured in the presence of SAG were subjected to *Tmsb10* KD (Supplementary Fig. 6). By contrast, *Tmsb4x* KD had no effect on ciliation (Supplementary Fig. 5d). Next, we examined whether ciliation and FLC differentiation were simultaneously suppressed by si*Tmsb10* in a dose-dependent manner. Testes were reconstructed with W-EGFP cells treated with increasing concentrations of si*Tmsb10*. As shown in Fig. 4c, FLC differentiation was suppressed dose dependently by si*Tmsb10*. Likewise, si*Tmsb10* dose-dependently decreased *Gli1* gene expression in cultured W-EGDFP cells (Fig. 4d).

We next attempted to determine the mechanism whereby *Tmsb10* regulates ciliogenesis. Regarding the function of TMSB10, experiments using human cancer cell lines showed that the protein binds directly to RAS, and thereby suppresses RAS-RAF interaction[30]. Moreover, this suppression ultimately resulted in failure of ERK phosphorylation and activation. Based on these findings, we planned to confirm the interaction between TMSB10 and RAS in W-EGFP cells with pull-down assays using ectopically expressed Flag-tagged TMSB10. Unfortunately, however, we could not find an efficient method for plasmid DNA transfection into W-EGFP cells. Thus, the interaction was confirmed in HEK293 cells (Fig. 4e). Subsequently, ERK phosphorylation, an event that occurs downstream of RAS/RAF activation, was examined in si*Cnt*- or si*Tmsb10*-treated W-EGFP cells. The amount of phosphorylated ERK (pERK) was increased by *Tmsb10* KD both in the presence and absence of SAG, whereas the amount of ERK was unaffected (Fig. 4f, g).

Taken together, these results indicated that TMSB10 promotes ciliogenesis and suppresses the RAS/ERK pathway. However, it remained unclear whether these two effects were connected. Several prior studies demonstrated that ciliogenesis was suppressed by the RAS/ERK pathway[44-46]. Therefore, as shown in Fig. 4h, we tentatively assumed that TMSB10 promotes ciliogenesis by suppressing the RAS/ERK pathway. To test this assumption, we examined the functional correlation between *Tmsb10* and *Ras* during FLC differentiation. W-EGFP cells treated with si*Tmsb10* and/or si*Ras* were used for testis reconstruction assays. Similar to the results shown in Fig. 3g and h, FLC differentiation was decreased by *Tmsb10* KD

(Fig. 4i). Consistent with the aforementioned assumption (Fig. 4h), FLC differentiation was increased by *Ras* KD. Moreover, the decrease in FLC differentiation by *Tmsb10* KD was canceled by simultaneous KD of *Ras*. The expression of the *Gli1* gene in cultured W-EGFP cells was similarly affected by treatment with these siRNAs (Fig. 4j).

We next examined the effect of *Ras* KD on ciliogenesis. Again, *Tmsb10* KD decreased the number of ciliated cells to 43% relative to control (Fig. 4k). Considering the effects of the KDs described above, we expected that *Ras* KD would increase the number of ciliated cells. Unexpectedly, however, this was not the case. As noted above, at most about 70% of W-EGFP cells were ciliated even when they were cultured in serum-free medium, suggesting that this was the maximum percentage that could be ciliated under this condition. This assumption seemed to be supported by a double-KD study with si*Tmsb10* and si*Ras*. Although KD of only *Ras* had no effect, the decrease of ciliated cells by *Tmsb10* KD was mitigated by *Ras* KD, and their numbers reached those seen following treatment with si*Cnt*.

PDGF possibly regulates ciliogenesis

As indicated in Fig. 4h, the RAS/ERK pathway seemed to be involved in FLC differentiation. However, it remained unclear which molecule(s) activated RAS in W-EGFP cells. We considered PDGF to be a possible candidate because FLC differentiation was largely abrogated by *Pdgfra* gene disruption[4], and PDGF signaling activated the RAS/ERK pathway[47].

First, we examined whether PDGF-AA activated FLC differentiation in reconstructed testes. As shown in Fig. 5a, FLC differentiation was not activated by PDGF-AA alone. Interestingly, however, PDGF-AA further enhanced the differentiation induced by SAG treatment. Likewise, *Gli1* gene expression was increased by PDGF-AA in the presence but not the absence of SAG (Fig. 5b).

Next, we examined whether PDGF affected ERK phosphorylation in W-EGFP cells. Consistent with previous studies[47], PDGF-AA increased the amount of pERK, although the amount of ERK was unchanged (Fig. 5c, d). SAG treatment had no effect on the amount of pERK. These results demonstrated that PDGF-AA increased pERK, probably by activating RAS. Since TMSB10 was shown to suppress the RAS/ERK pathway (Fig. 4f), it was expected that PDGF-promoted ERK phosphorylation would be increased by *Tmsb10* KD, and this was found to be the case (Fig. 5e, f). Based on these observations, it is likely that PDGF, in the presence of HH signaling, promotes FLC differentiation by activating the RAS/ERK pathway (Fig. 5g).

However, we noticed the following inconsistency. As described above, the RAS/ERK pathway was shown to suppress ciliogenesis[44-46]. In addition, the present study demonstrated that PDGF activated the RAS/ERK pathway in W-EGFP cells. These observations suggest that PDGF activates the RAS/ERK pathway and then suppresses ciliogenesis, resulting in suppression of DHH-dependent FLC differentiation (Fig. 5g). Nevertheless, Fig. 5a shows that PDGF promotes FLC differentiation cooperatively with DHH. This apparent inconsistency

strongly suggests that another pathway functions downstream of the PDGF receptor to modulate the suppression of ciliogenesis by the RAS/ERK pathway. In fact, ciliogenesis did not seem to be markedly affected by PDGF-AA (Fig. 5h).

Role of the PDGF-activated PI3K/AKT pathway in FLC differentiation

It has been established that PDGF signaling activates the PI3K/AKT pathway, in which PIP_3, which is generated from PIP_2 by PI3K, activates AKT (Fig. 6a)[47,48]. Thus, we investigated the possibility that this pathway regulates FLC differentiation by activating ciliogenesis. First, we examined whether AKT phosphorylation was promoted by PDGF-AA in W-EGFP cells. As expected, the amount of phosphorylated AKT was increased in the presence of PDGF-AA, whereas that of AKT was not affected (Fig. 6b, c). Next, we examined whether the PI3K/AKT pathway regulates FLC differentiation in testis reconstruction assays using W-EGFP cells treated with siRNA for *Akt* and *phosphatase and tensin homolog* (*Pten*). PTEN is known to suppress the PI3K/AKT pathway by mediating the conversion of PIP_3 to PIP_2 (Fig. 6a)[48]. When the reconstructed testes were incubated in the presence of SAG and PDGF-AA, *Akt* KD suppressed FLC differentiation. Conversely, *Pten* KD increased FLC differentiation (Fig. 6d). Likewise, the expression of *Gli1* in W-EGFP cells was decreased and increased by *Akt* KD and *Pten* KD, respectively (Fig. 6e). The *Tmsb10* KD-induced decreases in the FLC differentiation rate and in *Gli1* gene expression were observed in the presence of SAG and PDGF-AA.

We next examined the possible role of the PI3K/AKT pathway in the regulation of ciliogenesis. As shown in Fig. 6f, *Akt* KD decreased the number of ciliated W-EGFP cells in the presence of SAG and PDGF-AA. *Pten* KD was expected to increase the number of ciliated cells. However, as was the case with *Ras* KD (Fig. 4k), this increase was not observed.

Because several studies have demonstrated that activated AKT suppresses the RAS/ERK pathway by reducing RAF activity[49], we assumed that activating the PI3K/AKT pathway would reduce ERK phosphorylation and eventually promote FLC differentiation through ciliogenesis. Therefore, we examined whether inhibition of the PI3K/AKT pathway impacted ERK phosphorylation. As expected, the PI3K inhibitor wortmannin decreased AKT phosphorylation and increased ERK phosphorylation in W-EGFP cells (Fig. 6g, h). By contrast, when PI3K/AKT signaling was activated by *Pten* KD, AKT phosphorylation and ERK phosphorylation were increased and decreased, respectively (Fig. 6i, j). Together, these results suggest that activation of the PI3K/AKT pathway promotes FLC differentiation by enhancing ciliogenesis via suppression of the RAS/ERK pathway (Fig. 6a, Supplementary Fig. 7).

DISCUSSION

FLCs are known to increase in number in the fetal testes until late pregnancy, even though they rarely proliferate. Therefore, this increase has been thought to be due to the differentiation of progenitor cells into FLCs[13-19]. The interstitial space of the developing fetal testes is occupied predominantly by uncharacterized cells, in addition to smaller numbers of FLCs, peritubular myoid cells, endothelial cells, and macrophages. According to studies published so far, FLC progenitors are thought to be present in the interstitial space as cells positive for MAFB[14], ARX[7,13], and/or Notch[15,16] and Nestin[17]. In addition, our testis reconstruction study demonstrated the presence of FLC progenitors among the uncharacterized interstitial cells (W-EGFP cells) [34]. Based on these findings, it seemed critical to determine what kinds of cells constitute the uncharacterized W-EGFP cell population.

Identification of FLC progenitor cells by scRNA-seq

scRNA-seq is a powerful technique for characterizing cells that contain one or more unidentified cell populations. Indeed, novel cell populations have frequently been unveiled by this technique[50]. So far, studies have obtained single-cell transcriptomes from the cells constituting the fetal and postnatal testes[18,51-55]. These studies predicted the cellular lineages of FLCs and ALCs, as well as those of germ and Sertoli cells. Eventually, it was hypothesized that FLCs originate from uncharacterized interstitial cells. Unfortunately, however, none of the studies identified a particular cell population as segregating and differentiating into FLCs.

328 Although we currently do not know why these studies did not identify the cells that we found in
329 the present study, it might be because these single-cell studies utilized the overall population of
330 testicular cells, which included germ cells. Therefore, their contents demonstrate high biological
331 complexity, which might make it difficult to identify a population consisting of small number of
332 differentiating cells.

333 In contrast to these studies, Stevant *et al.* utilized EGFP-positive somatic cells from *Nr5a1*-
334 BAC-EGFP transgenic mice[18]. The developmental lineages of these cells were examined using
335 several stages of the developing testes (E10.5 to E16.5). Eventually, the authors identified
336 multipotent progenitor cells that gave rise to Sertoli and Leydig cells. Moreover, a recent study
337 by the same group demonstrated that *Wnt5a*-expressing cells in E11.5 to E12.5 testes were
338 potentially progenitors of both FLCs and ALCs[19].

339 Our current study utilized a simple cell population, namely W-EGFP cells, that probably
340 corresponds to uncharacterized interstitial cells. Ultimately, we identified FLC progenitor cells
341 characterized by the transient expression of *Tmsb10*. Utilization of a simple cell population may
342 have emphasized subtle differences and thereby enabled us to identify the small population of
343 FLC progenitors.

344 The developmental relation between progenitors characterized by *Wnt5a* versus *Tmsb10*
345 might be interesting. Considering that the expression of *Wnt5a* reaches a peak at E12.5-E13.5
346 and declines at E16.5[19], it might be reasonable to assume that the multipotent progenitor cells of
347 FLCs and ALCs are established at an early stage by the expression of *Wnt5a*. Thereafter, FLC

progenitors may be defined more selectively by the expression of *Tmsb10*. Because the cells used in the two studies with *Wnt5a* and *Tmsb10* were derived during distinct developmental stages, the studies might successfully identify progenitor cells at the distinct stages. Further investigations to determine the developmental relation between *Tmsb10*-positive and *Wnt5a*-positive cells, and also between previously identified *Mafb*-positive, *Arx*-positive, and *Notch*- and *Nestin*-positive cells might help us to clarify the entire process of FLCs differentiation.

Tmsb10 ***as a switch to promote FLC differentiation by suppressing the RAS/ERK pathway***

It is known that both *Tmsb10* and *Tmsb4x* possess actin sequestration activity, and thereby suppress actin polymerization[27,28]. *TMSB10* was found to be widely expressed in a variety of developing tissues, such as tooth germ[56], antler growth center[57], post-implantation embryos[25], ovarian follicles[58], and brain[59]. In addition, elevated expressions of TMSB10 were observed in a variety of cancers[29]. Because overexpression of TMSB10 resulted in the disappearance of F-actin and thereby enhanced migration and invasion activities[30], the functions of TMSB10 in cancers have been investigated based on the assumption that the protein acts as an actin-mediated tumor suppressor.

In addition, an interesting study published in 2005 showed that TMSB10 hindered RAS-RAF interaction, thereby suppressing the RAS/ERK signaling pathway as well as angiogenesis and tumor growth[30]. Consistent with these findings, another study indicated that TMSB10 reduced cancer cell activities by suppressing the ERK pathway[29]. Together, these studies

indicated that decreased expression of TMSB10 promotes tumor growth. In contrast, however, increased expression of TMSB10 was associated with high malignant potential in cancers[29]. Interestingly, a study of breast cancer revealed that enhanced expression of TMSB10 promoted proliferation and migration of cancer cells by activating AKT/FOXO signaling[60]. Although the functions of TMSB10 in cancer cells remain controversial, these findings regarding the potential of TMSB10 to regulate signal pathways showed that it has functions beyond those related to actin sequestration. In fact, our current study demonstrated that TMSB10 suppresses the RAS/ERK pathway in W-EGFP cells. Moreover, we found for the first time that *Tmsb10* promotes the differentiation of FLC progenitors.

Role of* Tmsb10 *in PDGF-DHH signal crosstalk through regulation of ciliation

PDGF plays crucial roles in the differentiation of various cell types by activating the RAS/ERK and PI3K/AKT pathways[47]. As for the functional correlation between the two pathways, it was found that the PI3K/AKT pathway may suppress the RAS/ERK pathway, and thus these two pathways exert opposing effects on cell differentiation[49]. Likewise, our present study demonstrated that PDGF can activate both the RAS/ERK and PI3K/AKT pathways, which suppress and promote FLC differentiation, respectively. This bidirectional activity of PDGF may maintain the balance between promotion and suppression of FLC differentiation, and thereby sustain the ability of some W-EGFP cells, if not all, to differentiate into FLCs.

It has been established that both DHH and PDGF are required for FLC differentiation[3,11,12]. However, it remains unclear whether these growth factors function cooperatively or independently in the differentiation process. Regarding this issue, our testis reconstruction assays fortunately showed that PDGF promotes FLC differentiation only in the presence of HH signaling. This finding strongly suggested the presence of crosstalk between PDGF and DHH signals. Eventually, we found that PDGF regulates the formation of cilia required for DHH signal transduction, confirming that crosstalk occurs between the two growth factors.

A previous study demonstrated crosstalk between PDGF and TGFβ during osteogenic differentiation[61]. Interestingly, the study showed that TGFβ-induced osteogenic differentiation was markedly enhanced by PDGF even though PDGF alone failed to promote the differentiation. Another study revealed that lens differentiation was regulated by antagonistic interaction between the PDGF-driven RAS/ERK pathway and the FGF-driven PI3K/AKT pathway[62]. In addition to the crosstalk between PDGF and both TGFβ and FGF, we revealed for the first time the presence of crosstalk between PDGF and HH signaling.

Our current study investigated *Tmsb10*, which was identified by single-cell transcriptome analyses of the uncharacterized interstitial cell population of the fetal testes, and provided several fundamental clues regarding the mechanism underlying FLC differentiation. To obtain a more comprehensive understanding of FLC differentiation, it might be critical to identify the mechanism whereby *Tmsb10* expression is selectively induced in a certain population of interstitial cells and how it is transiently expressed prior to differentiation into FLCs.

MATERIALS AND METHODS

Preparation of EGFP cells with strong (S-EGFP) or weak (W-EGFP) staining

We previously established *FLE-EGFP* mice using FLE (fetal Leydig enhancer) of the *Ad4BP/SF-1* gene[31]. EGFP-labeled transgenic testes were harvested at E16.5 and were dispersed with collagenase (Sigma-Aldrich, St. Louis, MO, USA) and dispase (Thermo Fisher Scientific, Waltham, MA, USA) as described previously[32]. Using JSAN (Bay bioscience, Kobe, Japan), the dispersed cells were fractionated by FACS into N-EGFP, W-EGFP, S-EGFP populations based on the negative, weak, or strong EGFP fluorescence intensity, respectively. All protocols for the animal experiments were approved by the Animal Care and Use Committee of Kyushu University, and all experiments were performed in accordance with the institutional guidelines.

scRNA-seq

Single S-EGFP or W-EGFP cells were plated by FACS (SH800, Sony, Tokyo, Japan) into individual wells of a 384-plate (Piko PCR Plate, Thermo Fisher Scientific) pre-loaded with lysis buffer. The CEL-Seq2 protocol established by Hashimshony *et al.* was used for RNA extraction and library preparation[35]. Briefly, the RNA of each cell was reverse transcribed using CEL-Seq primers containing an anchored poly(T), a 6-bp unique molecular identifier (UMI), a 5' Illumina adapter (San Diego, CA, USA), a cell-specific 6-bp barcode, and a T7 promoter (Supplementary Table 2). The External RNA Controls Consortium (ERCC) spike-ins (Thermo Fisher Scientific) were added to each preparation. After second-strand synthesis reaction, the double-stranded

cDNAs were transcribed *in vitro* by T7 RNA polymerase. The synthesized RNAs were reverse transcribed using random primers with the 3' Illumina adapter. Finally, the libraries were amplified by PCR (11 cycles). The pair-ended CEL-Seq2 libraries were sequenced by HiSeq 2500 (Illumina).

Data analysis of single-cell transcriptomes

The quality check of the raw sequence reads was performed using FastQC (version 0.11.7), and thereafter the reads were analyzed according to the CEL-Seq2 pipeline[35]. First, the reads of CEL-Seq2 libraries were demultiplexed to each cell using the CEL-Seq barcodes. To identify the transcript, the reads were mapped to the mouse reference genome (mm10) by Bowtie 2 software (version 2.3.4.1)[63]. PCR duplicates were removed using UMI information. The mapped reads were counted using HTSeq (version 0.9.1)[64]. The quality of the sequence data was further evaluated using a previously published method[65]; low-quality samples were removed by setting certain thresholds of low total reads, few expressed genes (< 1000 genes), and high spike-in proportions.

Cells in the G1 cell cycle phase were selected to avoid potential confounding effects from cell cycle-induced differences. Expression levels of the remaining genes were normalized and denoised. These data were subjected to hierarchical clustering on the significant principal components to divide cells into clusters. Differentially expressed genes (DEGs) of the clusters were identified to characterize the clusters. R packages including SingleCellExperiment

(version 1.0.0), scater (version 1.6.3), scran (version 1.6.9), Seurat (version 3.0.2), and Monocle (version 2.6.4) were used.

siRNA treatments

W-EGFP cells were cultured on Advanced TC 24-well plates (Greiner Bio-One, Kremsmünster, Austria) in α-modified Eagle's medium (α-MEM, Nacalai Tesque, Kyoto, Japan) supplemented with 10% fetal bovine serum (FBS, Thermo Fisher Scientific) and penicillin and streptomycin (PS, Thermo Fisher Scientific) at 37 °C under 5% CO_2 for 24 h. The cells were transfected with siRNAs using lipofectamine RNAiMAX reagent (Thermo Fisher Scientific) for 24 h. The siRNAs used in this study are listed in Supplementary Table 3. A control siRNA (Stealth RNAi Negative Control Medium GC Duplex; Thermo Fisher Scientific) was used as a negative control. The siRNA-treated cells were then utilized for qRT-PCR analyses, *in vitro* testis reconstruction, immunocytochemistry, and Western blotting. To investigate the effects of growth factor signals, the siRNA-treated cells were further cultured in the presence of SAG (0.5 μM; Adipogen Life Sciences, San Diego, CA, USA), mouse PDGF-AA (10 ng/mL; Sigma-Aldrich), wortmannin (0.1 μM; Cayman, Ann Arbor, MI, USA), or dimethyl sulfoxide (DMSO, Nacalai Tesque) as a negative control.

Immunostaining

Cryosections (10 μm) of mouse fetal testes and reconstructed testes attached to slide glasses were boiled for 5 min in 10 mM sodium citrate (pH 6.0) to unmask antigen epitopes[34]. The sections were incubated with primary antibodies in blocking buffer (2% skim milk (WAKO, Tokyo, Japan) in PBS) overnight at 4 °C, and subsequently with secondary antibodies in the blocking buffer for 1 h at room temperature. The primary and secondary antibodies used in this study are listed in Supplementary Table 4. Nuclei were counterstained with DAPI (Sigma-Aldrich).

To investigate ciliogenesis by immunofluorescence, W-EGFP cells cultured on μ-Plate 96-well TC (2.0×10^4 cells/well) (ibiTreat, ibidi, Martinsried, Germany) in the same medium as above for 24 h were treated with the siRNAs described above. After the siRNA treatment, the cells were cultured in this medium again for 24 h. Thereafter, they were fixed with 4% paraformaldehyde in PBS for 15 min at room temperature, and permeabilized with 0.5% Triton X-100 (WAKO) in PBS for 10 min followed by incubation in blocking buffer (1% skim milk in PBS) for 20 min at room temperature. Subsequently, the cells were treated with mouse anti-ARL13B antibody overnight at 4 °C, and then with Alexa Fluor 555-labeled goat anti-mouse IgG antibody for 1 h at room temperature (Supplementary Table 4). Nuclei were counterstained with DAPI.

Immunofluorescence images were captured using an LSM 700 confocal laser scanning microscope (Carl Zeiss, Jena, Germany) and a BZ-X700 fluorescence microscope (Keyence,

485 Osaka, Japan). The effects of the siRNA, SAG, and PDGF treatments on ciliogenesis were
486 evaluated as the percentage of ciliated cells in at least 500 overall cells in each sample (n = 5).
487
488 ***qRT-PCR analyses***
489 qRT-PCR was performed as previously described[66]. In brief, total RNAs (50 ng) prepared
490 using the RNeasy Micro Kit (Qiagen, Hilden, Germany) were reverse-transcribed to cDNA
491 using Moloney Murine Leukemia Virus reverse transcriptase (Thermo Fisher Scientific) and
492 random hexamers (Sigma-Aldrich). qRT-PCR was performed with a CFX96 Real-Time PCR
493 Detection System (Bio-Rad Laboratories, Hercules, CA, USA) using SYBR Select Master Mix
494 (Thermo Fisher Scientific). Gene expression was determined using the standard curve method.
495 Gene expression levels were normalized to those of *Rn18s* (*18S ribosomal RNA*). The primers
496 used for qRT-PCR are listed in Supplementary Table 5.
497
498 ***In vitro testis reconstruction***
499 Fetal testes were reconstructed as previously described[34,67]. Briefly, 8.0×10^5 whole
500 testicular cells prepared from wild-type fetal testes at E16.5 were mixed with W-EGFP cells
501 (2.0×10^4 cells) at E16.5 or W-EGFP cells treated with siRNA (2.5×10^4 cells). The
502 reconstructed testes were cultured on a V-shaped agarose gel for 2 days and then transferred
503 onto a bowl-shaped agarose gel, followed by culturing in α-MEM containing 10% Knockout
504 Serum Replacement (Thermo Fisher Scientific) and PS at 37 °C under 5% CO_2. To investigate

505 the effect of HH and PDGF signals on FLC differentiation, the reconstructed tissues were
506 treated with SAG (0.5 μM), mouse PDGF-AA (10 ng/mL), or DMSO. The reconstructed tissues
507 were observed under a BZ-X700 fluorescence microscope (Keyence) to capture EGFP-
508 fluorescent and bright-field images. The differentiation rate was calculated based on the EGFP-
509 positive area as previously described[68].
510
511 ***Western blotting analysis***
512 Whole-cell extracts were prepared from W-EGFP cells using lysis buffer (50 mM Tris–HCl
513 (pH 8.0), 50 mM NaCl, 1 mM EDTA, and 1% SDS) containing phosphatase inhibitors
514 (PhosSTOP tablet; Roche Diagnostics Corp., Indianapolis, IN, USA). After the protein
515 concentration was determined using a BCA Protein Assay Kit (Pierce Biotechnology, Rockford,
516 IL, USA), 5 μg of the whole-cell extract was subjected to SDS–polyacrylamide gel
517 electrophoresis, followed by electrophoretic transfer to polyvinylidene fluoride membranes
518 (Thermo Fisher Scientific). The membranes were incubated for 30 min at room temperature in
519 Blocking One (Nacalai Tesque). The membranes were treated with primary antibodies in a
520 reaction buffer (10% Blocking One in Tris-buffered saline; 10 mM Tris–HCl (pH 7.4), 150 mM
521 NaCl, 0.05% Tween 20) overnight at 4 °C, and thereafter with horseradish peroxidase-
522 conjugated secondary antibodies in the reaction buffer for 1 h at room temperature. The primary
523 and secondary antibodies used in this study are listed in Supplementary Table 6. Washed
524 membranes were developed using Chemi-Lumi One (Nacalai Tesque), and the images were

captured using a lumino image analyzer (ImageQuant LAS 500, GE Healthcare, Buckinghamshire, UK). All images were quantified using Image Lab 6.0 software (Bio-Rad).

Preparation of expression plasmids and a donor plasmid

Full-length cDNAs of *Tmsb10* and *Kras* was amplified by PCR with sets of primers (Supplementary Table 7), and were used to construct p3xFLAG-TMSB10 and pCMV-HA-KRAS expression plasmids, respectively. The p3xFLAG-CMV10 expression plasmid (Sigma-Aldrich) was used as a control study.

To construct a donor plasmid for CRISPR/Cas9 technology, an 849-bp fragment upstream from the first ATG and an 849-bp fragment downstream from the first ATG of the *Tmsb10* gene was amplified from the C57BL/6 genome. These fragments were used as the 5' and 3' homologous arms. *mCherry* tagged with human influenza hemagglutinin (HA) and Thoseaasigna virus 2A (T2A) at the N- and C-terminal sites (HA-mCherry-T2A), respectively, was synthesized as follows. A DNA fragment encoding *mCherry* was amplified from pmCherry-N1 (Clontech, Palo Alto, CA, USA) and inserted into the EcoRI/BglII site of pCMV-HA (Takara, Shiga, Japan) to generate pCMV-HA-mCherry. Thereafter, the plasmid was subjected to PCR with a 3' primer containing the T2A sequence to generate the HA-mCherry-T2A fragment. The primers used for amplification of the fragments are listed in Supplementary Table 7. Then, these three fragments (5' homologous arm, HA-mCherry-T2A, and 3'

544 homologous arm) were inserted into the SalI/EcoRI site of the pBluescript II KS+ using an In-
545 Fusion HD cloning kit (Clontech) (Supplementary Fig. 3).
546
547 ***Physical interaction between TMSB10 and KRAS***
548 p3xFLAG-TMSB10, p3xFLAG-CMV10, and pCMV-HA-KRAS were transfected using the
549 lipofectamine 2000 reagent (Thermo Fisher Scientific) in HEK 293 cells. The cells were lysed
550 in 50 mM Tris-HCl (pH 8.0), 300 mM NaCl, 10% glycerol, 1.5 mM $MgCl_2$, 1 mM EDTA, and
551 1% Triton X-100. The p3xFLAG-TMSB10 and p3xFLAG-CMV10 were immunoprecipitated
552 with anti-FLAG antibody-conjugated magnetic beads (Sigma-Aldrich), and then the beads were
553 sequentially washed three times with washing buffer (20 mM HEPES-KOH (pH 7.6), 100 mM
554 KCl, 10% glycerol,1 mM EDTA, and 0.05% Tween-20), and once with PBS. Finally, the
555 immunoprecipitates were eluted from the beads with 10 μl elution buffer (50 mM Tris-HCl (pH
556 7.4), 150 mM NaCl, 500 μg/ml FLAG peptide). Eluates and inputs were subjected to SDS-
557 polyacrylamide gel electrophoresis followed by Western blotting. The antibodies used in this
558 study are listed in Supplementary Table 6.
559
560 ***Generation of Tmsb10-mCherry knock-in mice***
561 A mouse line carrying the *mCherry* reporter gene at the *Tmsb10* locus (*Tmsb10-mCherry*
562 KI) was generated using CRISPR/Cas9 technology[69,70]. A guide RNA (gRNA) was designed to
563 target the transcription start site of *Tmsb10* using CRISPRdirect (http://crispr.dbcls.jp/). The

gRNA was synthesized and purified using a CUGA7 gRNA Synthesis Kit (Nippon Gene, Tokyo, Japan). Oocytes were collected from F1 hybrid (C57BL/6 x DBA/2) BDF1 female mice that were superovulated by standard procedures and fertilized *in vitro* with sperms from male mice of the same genetic background. CAS9 protein (100 ng/μl; Nippon Gene), the gRNA (250 ng/μl each), and the donor plasmid were microinjected into the cytoplasm on one side of the blastomere at the two-cell stage. The cells were transferred to pseudo-pregnant ICR female mice. Genotypes of the pups were analyzed by PCR. Nucleotide sequences of the primers for gRNA preparation and genotyping are shown in Supplementary Table 7. After backcrossing more than five times with C57BL/6J, *Tmsb10-mCherry* knock-in mice were further crossed with *FLE-EGFP* mice to generate *FLE-EGFP*;*Tmsb10-mCherry* mice. *FLE-EGFP* and *FLE-EGFP*;*Tmsb10-mCherry* male mice were crossed with ICR females (Japan SLC, Shizuoka, Japan).

Statistical analyses

At least three biologically independent samples were used in all experiments. All data are presented as mean ± standard error of the mean (SEM). We used Student's *t*-tests for comparisons between two groups, and one-way analysis of variance (ANOVA) followed by Tukey's multiple comparison test for multiple group comparisons. $p<0.05$ was considered to indicate statistically significant differences between groups. The statistical analyses were performed using R software version 3.6.3 (https://www.r-project.org).

584 **REFERENCES**

585 1 Svingen, T. & Koopman, P. Building the mammalian testis: origins, differentiation, and
586 assembly of the component cell populations. *Genes & development* **27**, 2409-2426,
587 doi:10.1101/gad.228080.113 (2013).

588 2 Zirkin, B. R. & Papadopoulos, V. Leydig cells: formation, function, and regulation.
589 *Biology of reproduction* **99**, 101-111, doi:10.1093/biolre/ioy059 (2018).

590 3 Yao, H. H., Whoriskey, W. & Capel, B. Desert Hedgehog/Patched 1 signaling specifies
591 fetal Leydig cell fate in testis organogenesis. *Genes & development* **16**, 1433-1440,
592 doi:10.1101/gad.981202 (2002).

593 4 Brennan, J., Tilmann, C. & Capel, B. Pdgfr-alpha mediates testis cord organization and
594 fetal Leydig cell development in the XY gonad. *Genes & development* **17**, 800-810,
595 doi:10.1101/gad.1052503 (2003).

596 5 Tang, H. *et al.* Notch signaling maintains Leydig progenitor cells in the mouse testis.
597 *Development* **135**, 3745-3753, doi:10.1242/dev.024786 (2008).

598 6 Sarraj, M. A. *et al.* Fetal Testis Dysgenesis and Compromised Leydig Cell Function in
599 Tgfbr3 (Betaglycan) Knockout Mice1. *Biology of reproduction* **82**, 153-162,
600 doi:10.1095/biolreprod.109.078766 (2010).

601 7 Kitamura, K. *et al.* Mutation of ARX causes abnormal development of forebrain and
602 testes in mice and X-linked lissencephaly with abnormal genitalia in humans. *Nature*
603 *genetics* **32**, 359-369, doi:10.1038/ng1009 (2002).

8 Cui, S. *et al.* Disrupted gonadogenesis and male-to-female sex reversal in Pod1 knockout mice. *Development* **131**, 4095-4105, doi:10.1242/dev.01266 (2004).

9 Buaas, F. W., Gardiner, J. R., Clayton, S., Val, P. & Swain, A. In vivo evidence for the crucial role of SF1 in steroid-producing cells of the testis, ovary and adrenal gland. *Development* **139**, 4561-4570, doi:10.1242/dev.087247 (2012).

10 Shima, Y. *et al.* Fetal Leydig cells dedifferentiate and serve as adult Leydig stem cells. *Development* **145**, doi:10.1242/dev.169136 (2018).

11 Barsoum, I. & Yao, H. H. Redundant and differential roles of transcription factors Gli1 and Gli2 in the development of mouse fetal Leydig cells. *Biology of reproduction* **84**, 894-899, doi:10.1095/biolreprod.110.088997 (2011).

12 Kothandapani, A. *et al.* GLI3 resides at the intersection of hedgehog and androgen action to promote male sex differentiation. *PLoS genetics* **16**, e1008810, doi:10.1371/journal.pgen.1008810 (2020).

13 Miyabayashi, K. *et al.* Aristaless related homeobox gene, Arx, is implicated in mouse fetal Leydig cell differentiation possibly through expressing in the progenitor cells. *PLoS one* **8**, e68050, doi:10.1371/journal.pone.0068050 (2013).

14 DeFalco, T., Takahashi, S. & Capel, B. Two distinct origins for Leydig cell progenitors in the fetal testis. *Developmental biology* **352**, 14-26, doi:10.1016/j.ydbio.2011.01.011 (2011).

15 Defalco, T., Saraswathula, A., Briot, A., Iruela-Arispe, M. L. & Capel, B. Testosterone levels influence mouse fetal Leydig cell progenitors through notch signaling. *Biology of reproduction* **88**, 91, doi:10.1095/biolreprod.112.106138 (2013).

16 Liu, C., Rodriguez, K. & Yao, H. H. Mapping lineage progression of somatic progenitor cells in the mouse fetal testis. *Development* **143**, 3700-3710, doi:10.1242/dev.135756 (2016).

17 Kumar, D. L. & DeFalco, T. A perivascular niche for multipotent progenitors in the fetal testis. *Nature communications* **9**, 4519, doi:10.1038/s41467-018-06996-3 (2018).

18 Stevant, I. *et al.* Deciphering Cell Lineage Specification during Male Sex Determination with Single-Cell RNA Sequencing. *Cell reports* **22**, 1589-1599, doi:10.1016/j.celrep.2018.01.043 (2018).

19 Ademi, H., Stévant, I., Rands, C. M., Conne, B. & Nef, S. Expression of *Wnt5a* defines the major progenitors of fetal and adult Leydig cells. *bioRxiv*, doi:10.1101/2020.07.25.221069 (2020).

20 Bangs, F. & Anderson, K. V. Primary Cilia and Mammalian Hedgehog Signaling. *Cold Spring Harbor perspectives in biology* **9**, doi:10.1101/cshperspect.a028175 (2017).

21 Hui, C. C. & Angers, S. Gli proteins in development and disease. *Annual review of cell and developmental biology* **27**, 513-537, doi:10.1146/annurev-cellbio-092910-154048 (2011).

642 22 Andrae, J., Gallini, R. & Betsholtz, C. Role of platelet-derived growth factors in
643 physiology and medicine. *Genes & development* **22**, 1276-1312,
644 doi:10.1101/gad.1653708 (2008).
645 23 Goldstein, A. L., Slater, F. D. & White, A. Preparation, assay, and partial purification of
646 a thymic lymphocytopoietic factor (thymosin). *Proceedings of the National Academy of*
647 *Sciences of the United States of America* **56**, 1010-1017, doi:10.1073/pnas.56.3.1010
648 (1966).
649 24 Lin, S. C. & Morrison-Bogorad, M. Developmental expression of mRNAs encoding
650 thymosins beta 4 and beta 10 in rat brain and other tissues. *Journal of molecular*
651 *neuroscience : MN* **2**, 35-44, doi: 10.1007/BF02896924 (1990).
652 25 Carpintero, P., Franco del Amo, F., Anadón, R. & Gómez-Márquez, J. Thymosin
653 beta10 mRNA expression during early postimplantation mouse development. *FEBS*
654 *letters* **394**, 103-106, doi:10.1016/0014-5793(96)00888-5 (1996).
655 26 Hannappel, E. beta-Thymosins. *Annals of the New York Academy of Sciences* **1112**, 21-
656 37, doi:10.1196/annals.1415.018 (2007).
657 27 Safer, D., Elzinga, M. & Nachmias, V. T. Thymosin beta 4 and Fx, an actin-
658 sequestering peptide, are indistinguishable. *The Journal of biological chemistry* **266**,
659 4029-4032 (1991).

28 Yu, F. X., Lin, S. C., Morrison-Bogorad, M., Atkinson, M. A. & Yin, H. L. Thymosin beta 10 and thymosin beta 4 are both actin monomer sequestering proteins. *The Journal of biological chemistry* **268**, 502-509 (1993).

29 Sribenja, S., Wongkham, S., Wongkham, C., Yao, Q. & Chen, C. Roles and mechanisms of beta-thymosins in cell migration and cancer metastasis: an update. *Cancer investigation* **31**, 103-110, doi:10.3109/07357907.2012.756111 (2013).

30 Lee, S. H. *et al.* Thymosin β 10 inhibits angiogenesis and tumor growth by interfering with Ras function. *Cancer research* **65**, 137-148 (2005).

31 Shima, Y. *et al.* Identification of an enhancer in the Ad4BP/SF-1 gene specific for fetal Leydig cells. *Endocrinology* **153**, 417-425, doi:10.1210/en.2011-1407 (2012).

32 Shima, Y. *et al.* Contribution of Leydig and Sertoli cells to testosterone production in mouse fetal testes. *Molecular endocrinology* **27**, 63-73, doi:10.1210/me.2012-1256 (2013).

33 Orth, J. M. Proliferation of Sertoli cells in fetal and postnatal rats: a quantitative autoradiographic study. *The Anatomical record* **203**, 485-492, doi:10.1002/ar.1092030408 (1982).

34 Inoue, M. *et al.* Isolation and Characterization of Fetal Leydig Progenitor Cells of Male Mice. *Endocrinology* **157**, 1222-1233, doi:10.1210/en.2015-1773 (2016).

35 Hashimshony, T. *et al.* CEL-Seq2: sensitive highly-multiplexed single-cell RNA-Seq. *Genome biology* **17**, 77, doi:10.1186/s13059-016-0938-8 (2016).

680 36 Nef, S. & Parada, L. F. Cryptorchidism in mice mutant for Insl3. *Nature genetics* **22**,
681 295-299, doi:10.1038/10364 (1999).
682 37 Zimmermann, S. *et al.* Targeted Disruption of the Insl3 Gene Causes Bilateral
683 Cryptorchidism. *Molecular endocrinology* **13**, 681-691, doi:10.1210/mend.13.5.0272
684 (1999).
685 38 Anderson, C. M. & Mendelson, C. R. Developmental and hormonal regulation of
686 cholesterol side chain cleavage cytochrome P-450 in the fetal rabbit testis. *Molecular*
687 *and cellular endocrinology* **55**, 121-130, doi:10.1016/0303-7207(88)90126-8 (1988).
688 39 O'Shaughnessy, P. J., Willerton, L. & Baker, P. J. Changes in Leydig cell gene
689 expression during development in the mouse. *Biology of reproduction* **66**, 966-975, doi:
690 10.1095/biolreprod66.4.966 (2002).
691 40 Morohashi, K., Baba, T. & Tanaka, M. Steroid hormones and the development of
692 reproductive organs. *Sexual development* **7**, 61-79, doi:10.1159/000342272 (2013).
693 41 Morohashi, K. I. & Omura, T. Ad4BP/SF-1, a transcription factor essential for the
694 transcription of steroidogenic cytochrome P450 genes and for the establishment of the
695 reproductive function. *FASEB journal* **10**, 1569-1577, doi:
696 10.1096/fasebj.10.14.9002548 (1996).
697 42 Parker, K. L. & Schimmer, B. P. Steroidogenic factor 1: a key determinant of endocrine
698 development and function. *Endocrine reviews* **18**, 361-377, doi:10.1210/edrv.18.3.0301
699 (1997).

43 Kasahara, K. & Inagaki, M. Primary ciliary signaling: links with the cell cycle. *Trends in cell biology* **31**, 954-964, doi:10.1016/j.tcb.2021.07.009 (2021).

44 Wang, S., Wei, Q., Dong, G. & Dong, Z. ERK-mediated suppression of cilia in cisplatin-induced tubular cell apoptosis and acute kidney injury. *Biochimica et biophysica acta* **1832**, 1582-1590, doi:10.1016/j.bbadis.2013.05.023 (2013).

45 Jenks, A. D. *et al.* Primary Cilia Mediate Diverse Kinase Inhibitor Resistance Mechanisms in Cancer. *Cell reports* **23**, 3042-3055, doi:10.1016/j.celrep.2018.05.016 (2018).

46 Kobayashi, T. *et al.* HDAC2 promotes loss of primary cilia in pancreatic ductal adenocarcinoma. *EMBO reports* **18**, 334-343, doi:10.15252/embr.201541922 (2017).

47 Ying, H. Z. *et al.* PDGF signaling pathway in hepatic fibrosis pathogenesis and therapeutics (Review). *Molecular medicine reports* **16**, 7879-7889, doi:10.3892/mmr.2017.7641 (2017).

48 Chalhoub, N. & Baker, S. J. PTEN and the PI3-kinase pathway in cancer. *Annual review of pathology* **4**, 127-150, doi:10.1146/annurev.pathol.4.110807.092311 (2009).

49 Rommel, C. *et al.* Differentiation stage-specific inhibition of the Raf-MEK-ERK pathway by Akt. *Science* **286**, 1738-1741, doi:10.1126/science.286.5445.1738 (1999).

50 Hwang, B., Lee, J. H. & Bang, D. Single-cell RNA sequencing technologies and bioinformatics pipelines. *Experimental & molecular medicine* **50**, 1-14, doi:10.1038/s12276-018-0071-8 (2018).

720 51 Green, C. D. *et al.* A Comprehensive Roadmap of Murine Spermatogenesis Defined by
721 Single-Cell RNA-Seq. *Developmental cell* **46**, 651-667.e610,
722 doi:10.1016/j.devcel.2018.07.025 (2018).
723 52 Hermann, B. P. *et al.* The Mammalian Spermatogenesis Single-Cell Transcriptome,
724 from Spermatogonial Stem Cells to Spermatids. *Cell reports* **25**, 1650-1667.e1658,
725 doi:10.1016/j.celrep.2018.10.026 (2018).
726 53 Lukassen, S., Bosch, E., Ekici, A. B. & Winterpacht, A. Single-cell RNA sequencing of
727 adult mouse testes. *Scientific data* **5**, 180192, doi:10.1038/sdata.2018.192 (2018).
728 54 Jung, M. *et al.* Unified single-cell analysis of testis gene regulation and pathology in
729 five mouse strains. *eLife* **8**, doi:10.7554/eLife.43966 (2019).
730 55 Tan, K., Song, H. W. & Wilkinson, M. F. Single-cell RNAseq analysis of testicular
731 germ and somatic cell development during the perinatal period. *Development* **147**,
732 doi:10.1242/dev.183251 (2020).
733 56 Shiotsuka, M. *et al.* The expression and function of thymosin beta 10 in tooth germ
734 development. *The International journal of developmental biology* **57**, 873-883,
735 doi:10.1387/ijdb.120240hs (2013).
736 57 Zhang, W. *et al.* Deer thymosin beta 10 functions as a novel factor for angiogenesis and
737 chondrogenesis during antler growth and regeneration. *Stem cell research & therapy* **9**,
738 166-166, doi:10.1186/s13287-018-0917-y (2018).

739 58 Salhab, M. *et al.* Thymosins β-4 and β-10 are expressed in bovine ovarian follicles and
740 upregulated in cumulus cells during meiotic maturation. *Reproduction, Fertility and*
741 *Development* **22**, 1206-1221, doi:10.1071/RD10015 (2010).
742 59 Anadón, R. *et al.* Differential expression of thymosins beta(4) and beta(10) during rat
743 cerebellum postnatal development. *Brain Research* **894**, 255-265, doi:10.1016/s0006-
744 8993(01)02024-8 (2001).
745 60 Zhang, X. *et al.* Thymosin beta 10 is a key regulator of tumorigenesis and metastasis
746 and a novel serum marker in breast cancer. *Breast Cancer Research* **19**, 15-15,
747 doi:10.1186/s13058-016-0785-2 (2017).
748 61 Yokota, J. *et al.* PDGF-induced PI3K-mediated signaling enhances the TGF-β-induced
749 osteogenic differentiation of human mesenchymal stem cells in a TGF-β-activated
750 MEK-dependent manner. *International journal of molecular medicine* **33**, 534-542,
751 doi:10.3892/ijmm.2013.1606 (2014).
752 62 Li, H. *et al.* Lens differentiation is controlled by the balance between PDGF and FGF
753 signaling. *PLoS biology* **17**, e3000133, doi:10.1371/journal.pbio.3000133 (2019).
754 63 Langmead, B. & Salzberg, S. L. Fast gapped-read alignment with Bowtie 2. *Nature*
755 *methods* **9**, 357-359, doi:10.1038/nmeth.1923 (2012).
756 64 Anders, S., Pyl, P. T. & Huber, W. HTSeq--a Python framework to work with high-
757 throughput sequencing data. *Bioinformatics* **31**, 166-169,
758 doi:10.1093/bioinformatics/btu638 (2015).

65 Lun, A. T., McCarthy, D. J. & Marioni, J. C. A step-by-step workflow for low-level analysis of single-cell RNA-seq data with Bioconductor. *F1000Research* **5**, 2122, doi:10.12688/f1000research.9501.2 (2016).

66 Yanai, S. *et al.* Gene expression and functional abnormalities in XX/Sry Leydig cells. *Scientific reports* **11**, 719, doi:10.1038/s41598-020-80741-z (2021).

67 Yokonishi, T. *et al.* In Vitro Reconstruction of Mouse Seminiferous Tubules Supporting Germ Cell Differentiation. *Biology of reproduction* **89** 1-6, doi:10.1095/biolreprod.113.108613 (2013).

68 Fukunaga, H. *et al.* High-precision microbeam radiotherapy reveals testicular tissue-sparing effects for male fertility preservation. *Scientific reports* **9**, 12618, doi:10.1038/s41598-019-48772-3 (2019).

69 Jinek, M. *et al.* A programmable dual-RNA-guided DNA endonuclease in adaptive bacterial immunity. *Science* **337**, 816-821, doi:10.1126/science.1225829 (2012).

70 Hara, S., Terao, M., Muramatsu, A. & Takada, S. Efficient production and transmission of CRISPR/Cas9-mediated mutant alleles at the IG-DMR via generation of mosaic mice using a modified 2CC method. *Scientific reports* **9**, 20202, doi:10.1038/s41598-019-56676-5 (2019).

Author contributions

M.I., T.B., Y.S., and K.-I.M. conceived, designed, and conducted the experiments, and performed data analyses. F.T. and Y.O. constructed the scRNA-seq libraries and obtained transcriptomes. M.I., S.Y., D.S., and M.S. analyzed the sequence data. M.T. and S.T. produced the genome-edited mice. K.S. and T.M. analyzed cell ciliation. M.I. and K.-I.M. prepared the manuscript.

Acknowledgements

We thank Dr. Junko Sasaki (Medical Research Institute, Tokyo Medical and Dental University) for her technical advice and discussion. We appreciate the technical assistance of The Research Support Center, Research Center for Human Disease Modeling, Kyushu University Graduate School of Medical Sciences. This work was supported by JSPS KAKENHI Grant Numbers JP20K08863 (T.B.), JP17H06427 (T.B., K.-I.M.), JP20H03436 (K.-I.M.), JP20H04935 (S.T.), JP19H05244 (Y.O.), JP20H00456 (Y.O.), JP20H04846 (Y.O.), and JP20K21398 (Y.O.); by JST CREST Grant Number JPMJCR16G1 (Y.O.); and by AMED under Grant Numbers JP20gk0210019 (K.-I.M.) and JP20ek0109489h0001 (Y.O.).

Author information

scRNA-seq data have been deposited in the DNA Data Bank of Japan under the accession code DRA013467 (http://trace.ddbj.nig.ac.jp/DRASearch/).

Figure legends

Figure 1. Characterization of S- and W-EGFP cells by scRNA-seq

(a) High-quality scRNA-seq datasets obtained from 80 S-EGFP and 341 W-EGFP cells were analyzed by hierarchical clustering. As indicated by the dendrogram (upper), the cells were divided into five cell clusters: cluster A (204 W-EGFP cells; light blue), cluster B (80 W-EGFP cells; blue), cluster C (57 W-EGFP cells; orange), cluster D (13 S-EGFP cells; green), and cluster E (67 S-EGFP cells; red). The heat map (lower) was based on genes in clusters C, D, and/or E whose expressions were altered. Genes differentially expressed in these clusters (group I to III) are shown. *Tmsb10* in group III is highlighted in red. ***(b, c)*** Results of t-SNE *(b)* and Monocle pseudo-time trajectory analyses *(c)* of the datasets are shown. The cellular distribution is shown (each dot represents one cell), with colors labeling the five clusters of cells as in *(a)*. ***(d-g)*** Expression levels of *Cyp11a1 (d)*, *Calr (e)*, *Tmsb10 (f)*, and *Arx (g)* in the cells above, as determined by scRNA-seq. Each dot represents one cell.

Figure 2. Increased expression of *Tmsb10* in putative FLC progenitors

(a) The testes of *FLE-EGFP*;*Tmsb10-mCherry* mouse fetuses at E16.5 were analyzed by immunofluorescence. Representative images of staining with EGFP (green), mCherry (red), and LAMININ (white), with all three stains overlaid in the image on the right. Arrows indicate cells double positive for mCherry and LAMININ. Closed arrowheads indicate cells double positive for mCherry (weakly stained) and EGFP. Open arrowheads indicate FLCs strongly stained with

EGFP. Asterisks mark testis tubules. Scale bar = 20 μm. ***(b-d)*** Expressions of *EGFP (b)*, *Tmsb10 (c)*, and *Pecam1 (d)* in N-EGFP (EGFP-negative, N, open bars), W-EGFP (W, light blue bars), and S-EGFP (S, blue bars) cells prepared from *FLE-EGFP* fetal testes at E16.5. The data were normalized by *Rn18s* and are presented as means ± SEM. Letters a, b, and c denote significant differences between the cell groups, N-EGFP (N), W-EGFP (W), and S-EGFP (S). $n = 3$. $p<0.01$.

Figure 3. Suppression of FLC differentiation by *Tmsb10* KD

(a) The experimental procedure for reconstruction of fetal testes. W-EGFP cells (E16.5) were plated and treated with siRNA for 24 h. Whole testicular cells prepared from wild-type fetuses (E16.5) were mixed with siRNA-treated W-EGFP cells to reconstruct testes. The detailed procedure for testis reconstruction and culture is described in the Materials and Methods. ***(b)*** A representative image of the reconstructed testis. Testicular tubules (tu) formed, and FLCs with strong EGFP staining were observed in the interstitial regions of the reconstructed testes. ***(c)*** The reconstructed testes were cultured in the presence (+) or absence (-) of SAG for 21 days. The reconstructed testes were examined under a fluorescence microscope to measure EGFP fluorescence. Scale bar = 100 μm. ***(d)*** The EGFP-positive cells (indicated by the relative EGFP-positive area) in the reconstructed testes above were analyzed quantitatively after incubation for 21 days. The cells were cultured in the absence (-, open bar) or presence of SAG (+, gray bar). $n = 3$. ***$p<0.001$. ***(e)*** Representative images of the reconstructed testes using W-EGFP cells treated with the following siRNAs: control (si*Cnt*), *Tmsb10* (si*T10*), *Tmsb4x* (si*T4x*), and

Ad4BP/SF-1 (si*Ad4*). Scale bar = 100 μm. ***(f)*** The EGFP-positive cells in the reconstructed testes above were analyzed quantitatively. Letters a, b, and c denote significant differences between the cell groups treated with si*Cnt*, si*T10*, si*T4x*, and si*Ad4*. $n = 3$. $p<0.001$. ***(g)*** Testes were reconstructed using W-EGFP cells treated with si*Cnt* or si*T10*. They were cultured for 21 days in the presence of SAG. Scale bar = 100 μm. ***(h)*** The EGFP-positive cells in the reconstructed testes above were analyzed quantitatively. $n = 3$. ***$p<0.001$. ***(i)*** W-EGFP cells were treated with si*Cnt* (open bar) or si*T10* (light blue bar). Expression of *Gli1* in the W-EGFP cells was examined by qRT-PCR. The data were normalized by *Rn18s* and are presented as means ± SEM. $n = 3$. **$p<0.01$.

Figure 4. Role of *Tmsb10* in the regulation of ciliogenesis via suppression of the RAS/ERK pathway

(a) E16.5 W-EGFP cells were treated with 0.1, 1.0, or 10.0 nM si*T10* or 10.0 nM *siCnt*, then cultured in serum-free medium for 24 h. Thereafter, the cells were subjected to immunostaining for the cilial marker protein ARL13B (red). Nuclei were stained with 4',6'-diamidino-2-phenylindole (DAPI) (blue). The enclosed area is enlarged at the top right. Arrows indicate primary cilia. Scale bar = 10 μm. ***(b)*** Ciliated cells detected in the studies above were counted. The ratios of the ciliated cells to all cells (%) are shown. $n = 5$. *$p<0.001$. ***(c)*** W-EGFP cells were treated with 0.1, 1.0, or 10.0 nM si*T10* or 10.0 nM *siCnt*, then subjected to testis reconstruction assay. The EGFP-positive cells (indicated by the relative EGFP-positive area) in the reconstructed

855 testes were analyzed quantitatively after incubation for 21 days. $n = 3$. $p<0.001$. ***(d)*** W-EGFP
856 cells were cultured and treated with 0.1, 1.0, or 10.0 nM si*T10* or 10.0 nM si*Cnt*. Expression of
857 the *Gli1* gene in the cells was examined. The data were standardized using *Rn18s*. $n = 3$. $p<0.001$.
858 ***(e)*** Interactions between TMSB10 and RAS were examined. Whole-cell lysates were prepared
859 from HEK293 cells overexpressing FLAG-TMSB10 or FLAG together with KRAS. Proteins
860 interacting with TMSB10 were immunoprecipitated with anti-FLAG antibody. The
861 immunoprecipitates were subjected to immunoblotting using antibodies for pan-RAS and FLAG.
862 The positions of molecular weight markers are indicated at the left. Full blot images are displayed
863 in Supplemental Fig. 8. ***(f)*** Whole-cell extracts were prepared from E16.5 W-EGFP cells treated
864 with si*T10* or si*Cnt* in the presence (+) or absence (-) of SAG. Levels of phospho-ERK (pERK)
865 and ERK were examined by Western blotting. ***(g)*** Signal intensities in the blots above were
866 quantified as described in the Materials and Methods. The amounts of pERK relative to ERK are
867 shown. $n = 3$. $p<0.01$. ***(h)*** A schematic illustration summarizing the results so far. TMSB10 was
868 assumed to suppress the RAS/ERK pathway by interacting with RAS. ***(i)*** W-EGFP cells were
869 treated with si*Cnt* (open bar), si*T10* (light blue bar), si*Ras* (dark blue bar), or both si*T10* and si*Ras*
870 (red bar). These cells were then used for testis reconstruction. The reconstructed testes were
871 cultured in the presence of SAG for 21 days. The EGFP-positive cells in the reconstructed testes
872 were analyzed quantitatively. $n = 3$. $p<0.001$. ***(j)*** W-EGFP cells were treated with siRNAs as
873 above and then cultured in the presence of SAG. The expression of *Gli1* was examined by qRT-
874 PCR. The data were standardized using *Rn18s*. $n = 3$. $p<0.001$. ***(k)*** W-EGFP cells were treated

875 with siRNAs as above, and their effect on ciliogenesis was examined by immunostaining for
876 ARL13B. Ciliated cells were counted and the ratios of these cells to all cells (%) are plotted. n =
877 5. *p<0.001. Letters a, b, and c on the bars in *(c)*, *(d)*, *(g)*, *(i)*, and *(j)* denote significant differences
878 between the cell groups.
879
880 **Figure 5. Activation of the RAS/ERK pathway by PDGF**
881 ***(a)*** Reconstructed testes were incubated in the absence (open bar) or presence of PDGF-AA
882 (green bar), SAG (dark blue bar), or both PDGF-AA and SAG (red bar). The EGFP-positive cells
883 in the reconstructed testes were analyzed quantitatively after incubation for 21 days. n = 3.
884 p<0.001. ***(b)*** W-EGFP cells were cultured under the same conditions as above. Expression of *Gli1*
885 in the cells was examined by qRT-PCR. The data were normalized by *Rn18s* and are presented
886 as means ± SEM. n = 3. p<0.01. ***(c)*** Whole-cell extracts prepared from W-EGFP cells were
887 cultured in the presence (+) or absence (-) of PDGF-AA and subjected to Western blotting for
888 ERK and pERK. The position of a molecular weight marker is indicated at the left. ***(d)*** Signal
889 intensities of the blots above were quantified as described in the Materials and Methods. The
890 amounts of pERK relative to ERK are shown. Letters a, b, and c on the bars in *(a)*, *(b)*, and *(d)*
891 denote significant differences between the cell groups. n = 3. p<0.01. ***(e)*** W-EGFP cells were
892 treated with siRNA for si*T10* and thereafter cultured in the presence (+) or absence (-) of PDGF-
893 AA. Whole-cell extracts prepared from the cells were subjected to Western blotting for ERK and
894 pERK. ***(f)*** Signal intensities of the blots above were quantified. The amounts of pERK relative to

ERK are shown. $n = 3$. ***$p<0.001$. Full blot images for (c) and (d) are displayed in Supplemental Fig. 8. ***(g)*** A tentative schema for the function of PDGF is shown. It was assumed that another signal pathway could be activated downstream of PDGF. ***(h)*** W-EGFP cells were cultured in the absence (-) or presence (+) of PDGF-AA and SAG. Ciliogenesis in the W-EGFP cells was examined by immunostaining for ARL13B. Ciliated cells were counted and the ratios of these cells to all cells (%) are plotted. $n = 3$. *$p<0.001$.

Figure 6. Dual role of PDGF in regulating FLC differentiation

(a) A schematic summary of signal pathways regulating FLC differentiation and in which *Tmsb10* acts as a suppressor. ***(b)*** W-EGFP cells were cultured in the presence (+) or absence (-) of PDGF-AA. Whole-cell extracts prepared from the cells were subjected to Western blotting for phospho-AKT (pAKT) and AKT. Representative images of the blots are shown. The positions of molecular weight markers are indicated at the left. ***(c)*** Signal intensities in the blots above were quantified as described in the Materials and Methods. The amounts of pAKT relative to AKT are shown. $n = 3$. *$p<0.05$. ***(d)*** W-EGFP cells were treated with si*Cnt*, si*T10*, si*Akt*, or si*Pten*, and then used for testis reconstruction. The reconstructed testes were cultured in the presence of SAG and PDGF for 21 days. The EGFP-positive cells in the reconstructed testes were quantified. $n = 3$. $p<0.001$. ***(e)*** W-EGFP cells were cultured under the same conditions as above. Expression of *Gli1* in the cells was determined by qRT-PCR. The data were normalized by *Rn18s* and are presented as means ± SEM. $n = 3$. $p<0.001$. Letters a, b, and c on the bars in *(d)* and *(e)* denote significant

915 differences. ***(f)*** W-EGFP cells were cultured under the same conditions as above. Ciliogenesis in
916 the W-EGFP cells was examined by immunostaining for ARL13B. $n = 5$. *$p<0.001$. ***(g)*** W-EGFP
917 cells were cultured in the presence (+) or absence (-) of wortmannin (Wort). Whole-cell extracts
918 were subjected to Western blotting for pAKT, AKT, pERK, and ERK. ***(h)*** Signal intensities in
919 the blots above were quantified as described in the Materials and Methods. The amounts of pAKT
920 relative to AKT (left) and pERK relative to ERK (right) are shown. $n = 3$. **$p<0.01$. ***$p<0.001$.
921 ***(i)*** W-EGFP cells treated with siRNA for si*Pten* and si*Cnt*. Whole-cell extracts prepared from the
922 cells were subjected to Western blotting for pAKT, AKT, pERK, and ERK. Full blot images for
923 *(b)*, *(g)*, and *(i)* are shown in Supplemental Fig. 8. ***(j)*** Signal intensities in the blots above were
924 quantified. The amounts of pAKT relative to AKT (left) and pERK relative to ERK (right) are
925 shown. $n = 3$. *$p<0.05$. **$p<0.01$.

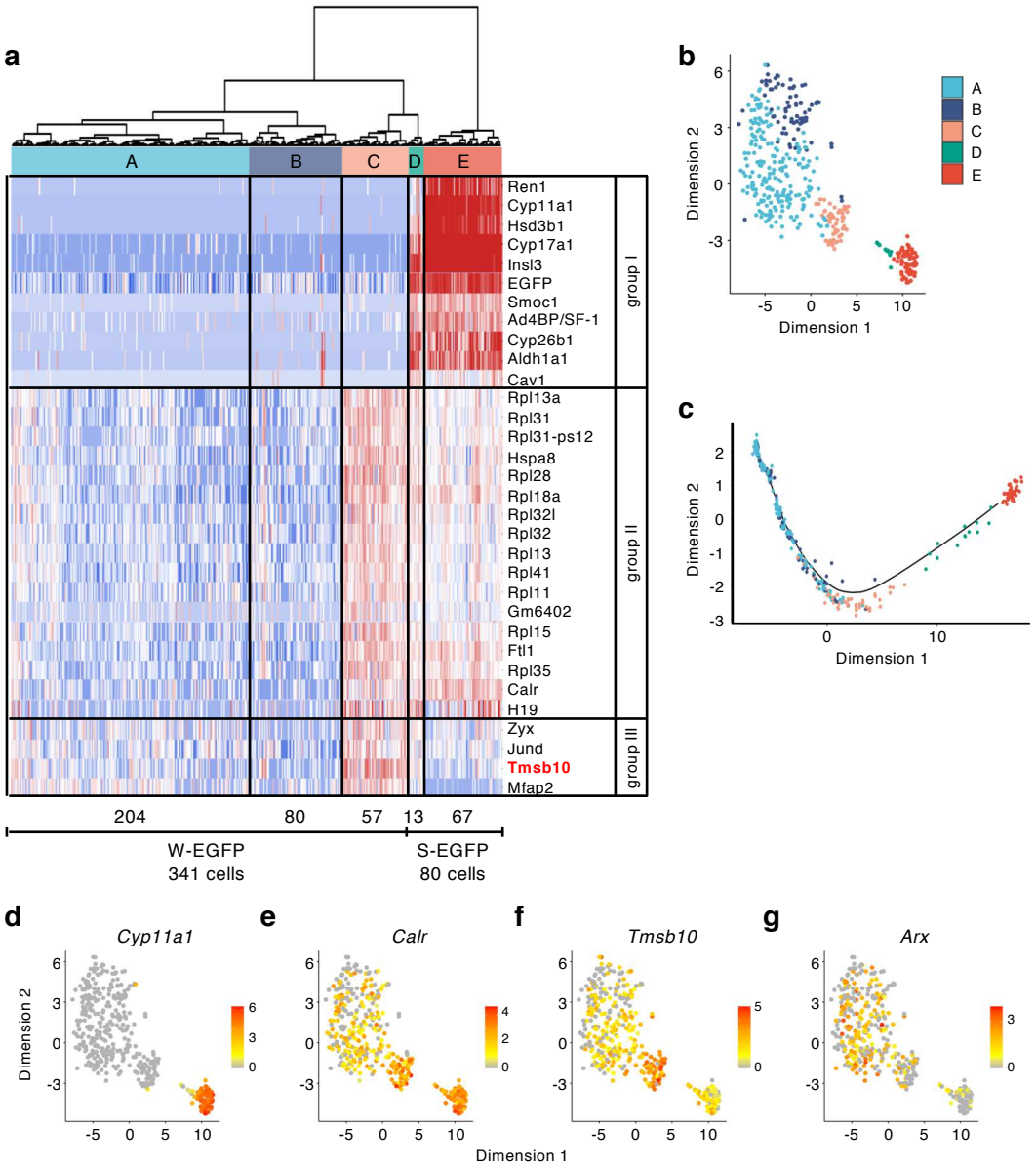

Figure 1. Characterization of S- and W-EGFP cells by scRNA-seq

(a) High-quality scRNA-seq datasets obtained from 80 S-EGFP and 341 W-EGFP cells were analyzed by hierarchical clustering. As indicated by the dendrogram (upper), the cells were divided into five cell clusters: cluster A (204 W-EGFP cells; light blue), cluster B (80 W-EGFP cells; blue), cluster C (57 W-EGFP cells; orange), cluster D (13 S-EGFP cells; green), and cluster E (67 S-EGFP cells; red). The heat map (lower) was based on genes in clusters C, D, and/or E whose expressions were altered. Genes differentially expressed in these clusters (group I to III) are shown. *Tmsb10* in group III is highlighted in red. ***(b, c)*** Results of t-SNE *(b)* and Monocle pseudo-time trajectory analyses *(c)* of the datasets are shown. The cellular distribution is shown (each dot represents one cell), with colors labeling the five clusters of cells as in *(a)*. ***(d-g)*** Expression levels of *Cyp11a1 (d)*, *Calr (e)*, *Tmsb10 (f)*, and *Arx (g)* in the cells above, as determined by scRNA-seq. Each dot represents one cell.

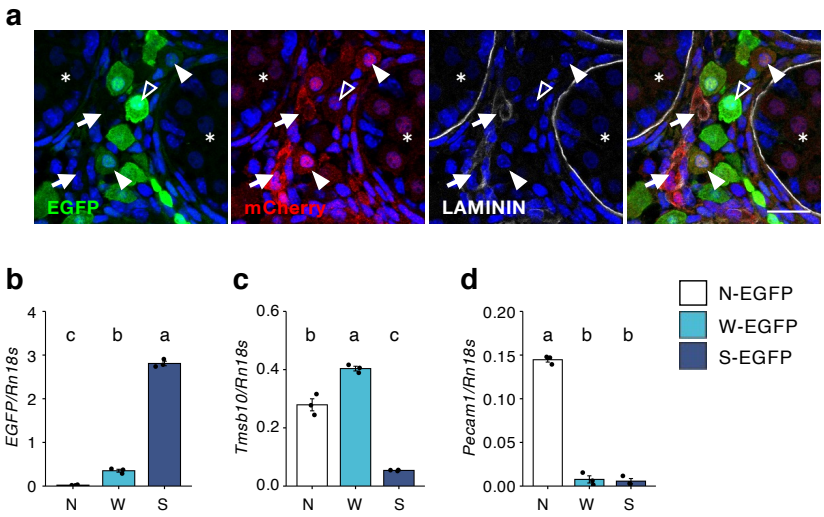

Figure 2. Increased expression of *Tmsb10* in putative FLC progenitors

(a) The testes of *FLE-EGFP*;*Tmsb10-mCherry* mouse fetuses at E16.5 were analyzed by immunofluorescence. Representative images of staining with EGFP (green), mCherry (red), and LAMININ (white), with all three stains overlaid in the image on the right. Arrows indicate cells double positive for mCherry and LAMININ. Closed arrowheads indicate cells double positive for mCherry (weakly stained) and EGFP. Open arrowheads indicate FLCs strongly stained with EGFP. Asterisks mark testis tubules. Scale bar = 20 μm. ***(b-d)*** Expressions of *EGFP (b)*, *Tmsb10 (c)*, and *Pecam1 (d)* in N-EGFP (EGFP-negative, N, open bars), W-EGFP (W, light blue bars), and S-EGFP (S, blue bars) cells prepared from *FLE-EGFP* fetal testes at E16.5. The data were normalized by *Rn18s* and are presented as means $\pm$ SEM. Letters a, b, and c denote significant differences between the cell groups, N-EGFP (N), W-EGFP (W), and S-EGFP (S). $n = 3$. $p<0.01$.

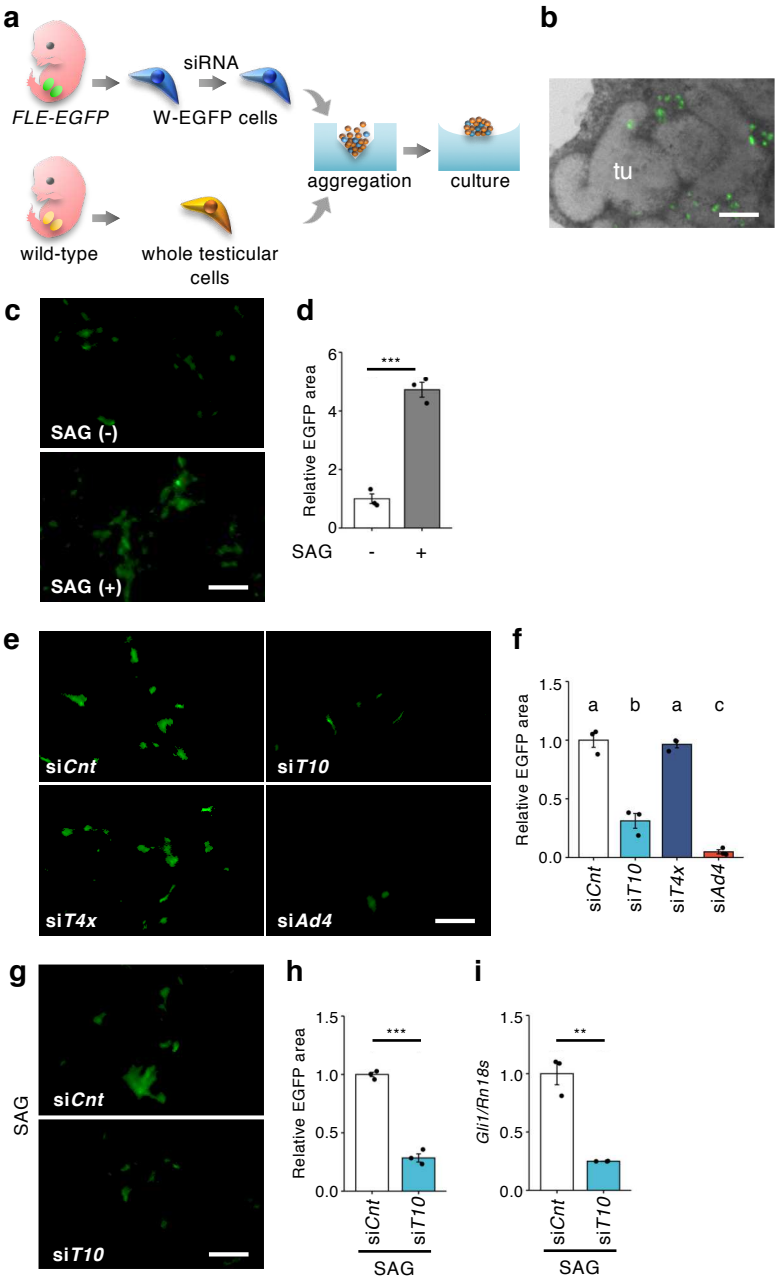
a
FLE-EGFP
siRNA
W-EGFP cells
aggregation
culture
wild-type
whole testicular cells
b
tu
c
SAG (-)
SAG (+)
d
Relative EGFP area
***
SAG
e
siCnt
siT10
siT4x
siAd4
f
Relative EGFP area
a
b
a
c
siCnt
siT10
siT4x
siAd4
g
SAG
siCnt
siT10
h
Relative EGFP area
***
siCnt
siT10
SAG
i
Gli1/Rn18s
**
siCnt
siT10
SAG

Figure 3. Suppression of FLC differentiation by *Tmsb10* KD

(a) The experimental procedure for reconstruction of fetal testes. W-EGFP cells (E16.5) were plated and treated with siRNA for 24 h. Whole testicular cells prepared from wild-type fetuses (E16.5) were mixed with siRNA-treated W-EGFP cells to reconstruct testes. The detailed procedure for testis reconstruction and culture is described in the Materials and Methods. ***(b)*** A representative image of the reconstructed testis. Testicular tubules (tu) formed, and FLCs with strong EGFP staining were observed in the interstitial regions of the reconstructed testes. ***(c)*** The reconstructed testes were cultured in the presence (+) or absence (-) of SAG for 21 days. The reconstructed testes were examined under a fluorescence microscope to measure EGFP fluorescence. Scale bar = 100 μm. ***(d)*** The EGFP-positive cells (indicated by the relative EGFP-positive area) in the reconstructed testes above were analyzed quantitatively after incubation for 21 days. The cells were cultured in the absence (-, open bar) or presence of SAG (+, gray bar). $n = 3$. ***$p<0.001$. ***(e)*** Representative images of the reconstructed testes using W-EGFP cells treated with the following siRNAs: control (si*Cnt*), *Tmsb10* (si*T10*), *Tmsb4x* (si*T4x*), and *Ad4BP/SF-1* (si*Ad4*). Scale bar = 100 μm. ***(f)*** The EGFP-positive cells in the reconstructed testes above were analyzed quantitatively. Letters a, b, and c denote significant differences between the cell groups treated with si*Cnt*, si*T10*, si*T4x*, and si*Ad4*. $n = 3$. $p<0.001$. ***(g)*** Testes were reconstructed using W-EGFP cells treated with si*Cnt* or si*T10*. They were cultured for 21 days in the presence of SAG. Scale bar = 100 μm. ***(h)*** The EGFP-positive cells in the reconstructed testes above were analyzed quantitatively. $n = 3$. ***$p<0.001$. ***(i)*** W-EGFP cells were treated with si*Cnt* (open bar) or si*T10* (light blue bar). Expression of *Gli1* in the W-EGFP cells was examined by qRT-PCR. The data were normalized by *Rn18s* and are presented as means ± SEM. $n = 3$. **$p<0.01$.

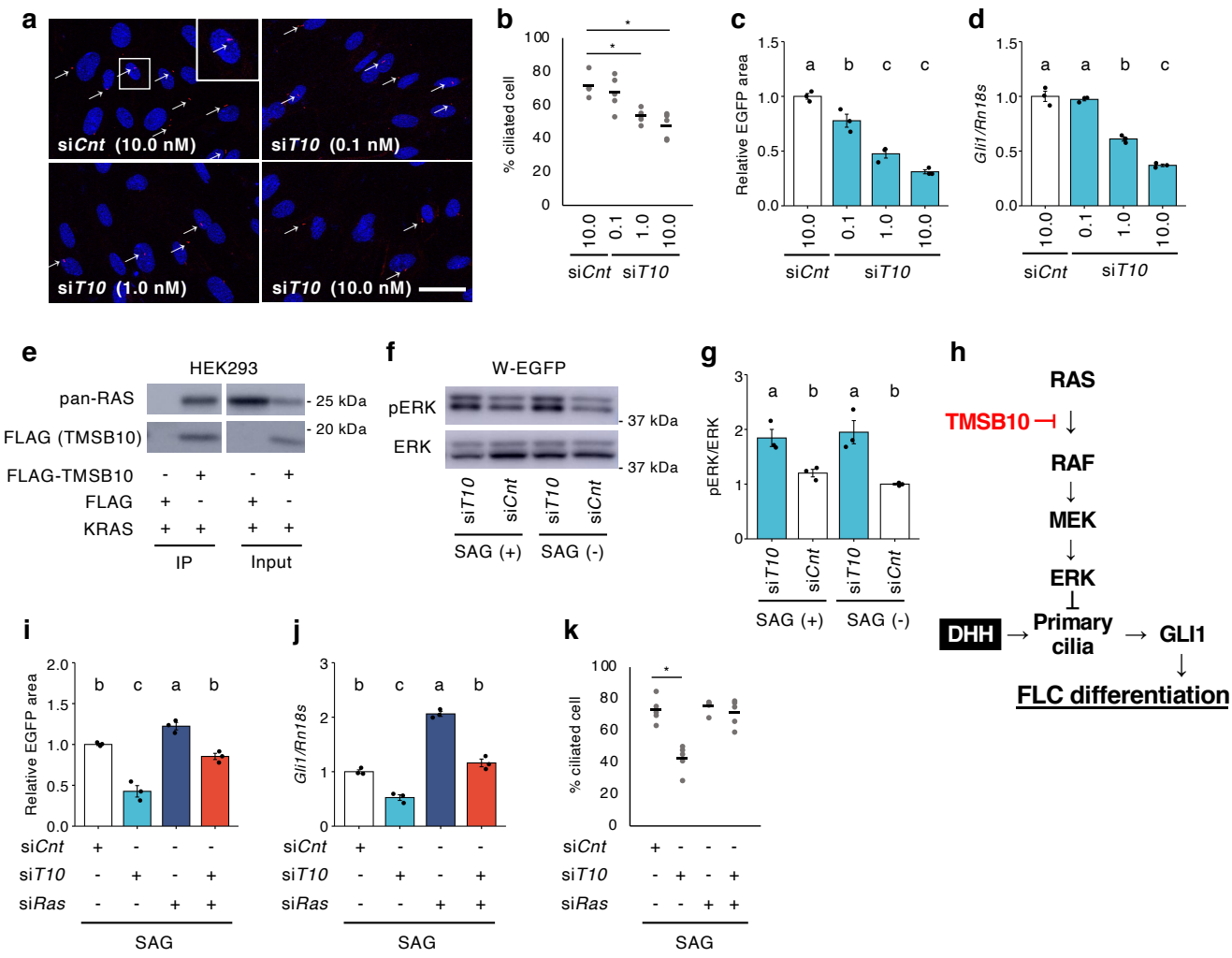
a
siCnt (10.0 nM)
siT10 (0.1 nM)
siT10 (1.0 nM)
siT10 (10.0 nM)
b
% ciliated cell
siCnt siT10
c
Relative EGFP area
d
Gli1/Rn18s
e
HEK293
pan-RAS
FLAG (TMSB10)
25 kDa
20 kDa
FLAG-TMSB10
FLAG
KRAS
IP
Input
f
W-EGFP
pERK
ERK
37 kDa
SAG (+)
SAG (-)
g
pERK/ERK
h
RAS
TMSB10
RAF
MEK
ERK
DHH
Primary cilia
GLI1
FLC differentiation
i
Relative EGFP area
siCnt
siT10
siRas
SAG
j
Gli1/Rn18s
k
% ciliated cell

Figure 4. Role of *Tmsb10* in the regulation of ciliogenesis via suppression of the RAS/ERK pathway

(a) E16.5 W-EGFP cells were treated with 0.1, 1.0, or 10.0 nM si*T10* or 10.0 nM *siCnt*, then cultured in serum-free medium for 24 h. Thereafter, the cells were subjected to immunostaining for the cilial marker protein ARL13B (red). Nuclei were stained with 4',6'-diamidino-2-phenylindole (DAPI) (blue). The enclosed area is enlarged at the top right. Arrows indicate primary cilia. Scale bar = 10 μm. ***(b)*** Ciliated cells detected in the studies above were counted. The ratios of the ciliated cells to all cells (%) are shown. $n = 5$. *$p<0.001$. ***(c)*** W-EGFP cells were treated with 0.1, 1.0, or 10.0 nM si*T10* or 10.0 nM *siCnt*, then subjected to testis reconstruction assay. The EGFP-positive cells (indicated by the relative EGFP-positive area) in the reconstructed testes were analyzed quantitatively after incubation for 21 days. $n = 3$. $p<0.001$. ***(d)*** W-EGFP cells were cultured and treated with 0.1, 1.0, or 10.0 nM si*T10* or 10.0 nM si*Cnt*. Expression of the *Gli1* gene in the cells was examined. The data were standardized using *Rn18s*. $n = 3$. $p<0.001$. ***(e)*** Interactions between TMSB10 and RAS were examined. Whole-cell lysates were prepared from HEK293 cells overexpressing FLAG-TMSB10 or FLAG together with KRAS. Proteins interacting with TMSB10 were immunoprecipitated with anti-FLAG antibody. The immunoprecipitates were subjected to immunoblotting using antibodies for pan-RAS and FLAG. The positions of molecular weight markers are indicated at the left. Full blot images are displayed in Supplemental Fig. 8. ***(f)*** Whole-cell extracts were prepared from E16.5 W-EGFP cells treated with si*T10* or si*Cnt* in the presence (+) or absence (-) of SAG. Levels of phospho-ERK (pERK) and ERK were examined by Western blotting. ***(g)*** Signal intensities in the blots above were quantified as described in the Materials and Methods. The amounts of pERK relative to ERK are shown. $n = 3$. $p<0.01$. ***(h)*** A schematic illustration summarizing the results so far. TMSB10 was assumed to suppress the RAS/ERK pathway by interacting with RAS. ***(i)*** W-EGFP cells were treated with si*Cnt* (open bar), si*T10* (light blue bar), si*Ras* (dark blue bar), or both si*T10* and si*Ras* (red bar). These cells were then used for testis reconstruction. The reconstructed testes were cultured in the presence of SAG for 21 days. The EGFP-positive cells in the reconstructed testes were analyzed quantitatively. $n = 3$. $p<0.001$. ***(j)*** W-EGFP cells were treated with siRNAs as above and then cultured in the presence of SAG. The expression of *Gli1* was examined by qRT-PCR. The data were standardized using *Rn18s*. $n = 3$. $p<0.001$. ***(k)*** W-EGFP cells were treated with siRNAs as above, and their effect on ciliogenesis was examined by immunostaining for ARL13B. Ciliated cells were counted and the ratios of these cells to all cells (%) are plotted. $n = 5$. *$p<0.001$. Letters a, b, and c on the bars in *(c)*, *(d)*, *(g)*, *(i)*, and *(j)* denote significant differences between the cell groups.

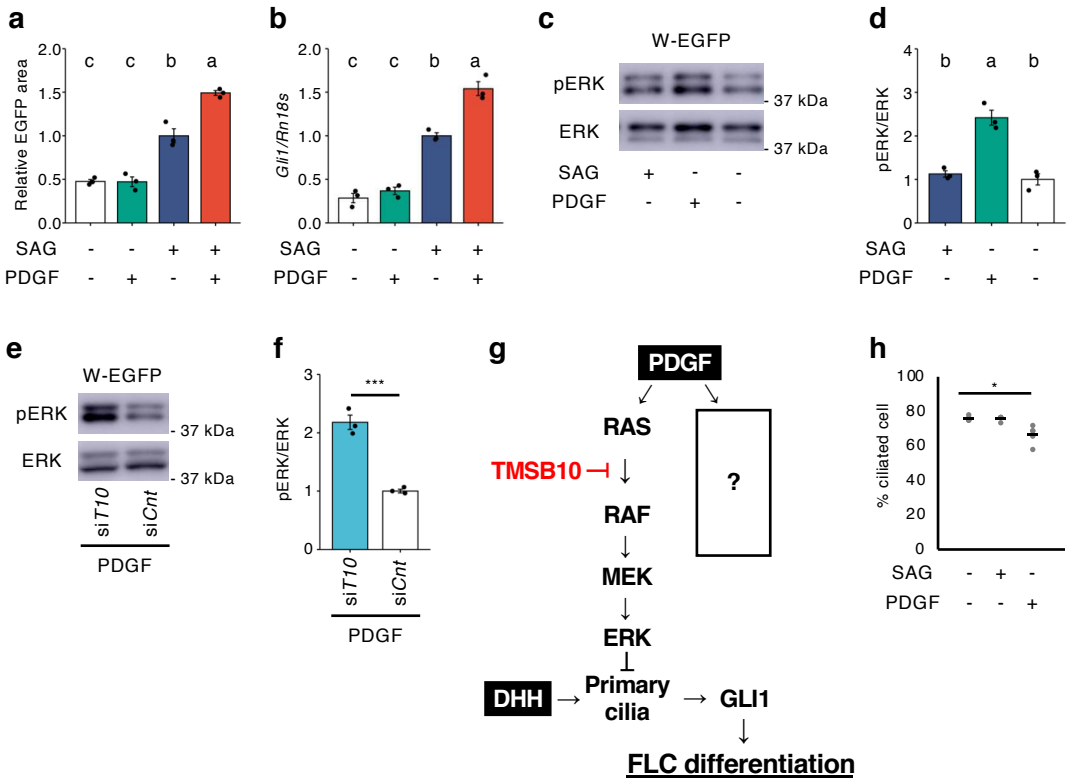
a
Relative EGFP area
2.0
1.5
1.0
0.5
0.0
c c b a
SAG - - + +
PDGF - + - +
b
Gli1/Rn18s
2.0
1.5
1.0
0.5
0.0
c c b a
SAG - - + +
PDGF - + - +
c
W-EGFP
pERK
ERK
37 kDa
37 kDa
SAG + - -
PDGF - + -
d
pERK/ERK
4
3
2
1
0
b a b
SAG + - -
PDGF - + -
e
W-EGFP
pERK
ERK
37 kDa
37 kDa
siT10
siCnt
PDGF
f
pERK/ERK
3
2
1
0
***
siT10
siCnt
PDGF
g
PDGF
RAS
TMSB10
RAF
MEK
ERK
?
DHH
Primary cilia
GLI1
FLC differentiation
h
% ciliated cell
100
80
60
40
20
0
*
SAG - + -
PDGF - - +

Figure 5. Activation of the RAS/ERK pathway by PDGF

(a) Reconstructed testes were incubated in the absence (open bar) or presence of PDGF-AA (green bar), SAG (dark blue bar), or both PDGF-AA and SAG (red bar). The EGFP-positive cells in the reconstructed testes were analyzed quantitatively after incubation for 21 days. $n = 3$. $p<0.001$. ***(b)*** W-EGFP cells were cultured under the same conditions as above. Expression of *Gli1* in the cells was examined by qRT-PCR. The data were normalized by *Rn18s* and are presented as means ± SEM. $n = 3$. $p<0.01$. ***(c)*** Whole-cell extracts prepared from W-EGFP cells were cultured in the presence (+) or absence (-) of PDGF-AA and subjected to Western blotting for ERK and pERK. The position of a molecular weight marker is indicated at the left. ***(d)*** Signal intensities of the blots above were quantified as described in the Materials and Methods. The amounts of pERK relative to ERK are shown. Letters a, b, and c on the bars in *(a)*, *(b)*, and *(d)* denote significant differences between the cell groups. $n = 3$. $p<0.01$. ***(e)*** W-EGFP cells were treated with siRNA for si*T10* and thereafter cultured in the presence (+) or absence (-) of PDGF-AA. Whole-cell extracts prepared from the cells were subjected to Western blotting for ERK and pERK. ***(f)*** Signal intensities of the blots above were quantified. The amounts of pERK relative to ERK are shown. $n = 3$. $^{***}p<0.001$. Full blot images for (c) and (d) are displayed in Supplemental Fig. 8. ***(g)*** A tentative schema for the function of PDGF is shown. It was assumed that another signal pathway could be activated downstream of PDGF. ***(h)*** W-EGFP cells were cultured in the absence (-) or presence (+) of PDGF-AA and SAG. Ciliogenesis in the W-EGFP cells was examined by immunostaining for ARL13B. Ciliated cells were counted and the ratios of these cells to all cells (%) are plotted. $n = 3$. $^{*}p<0.001$.

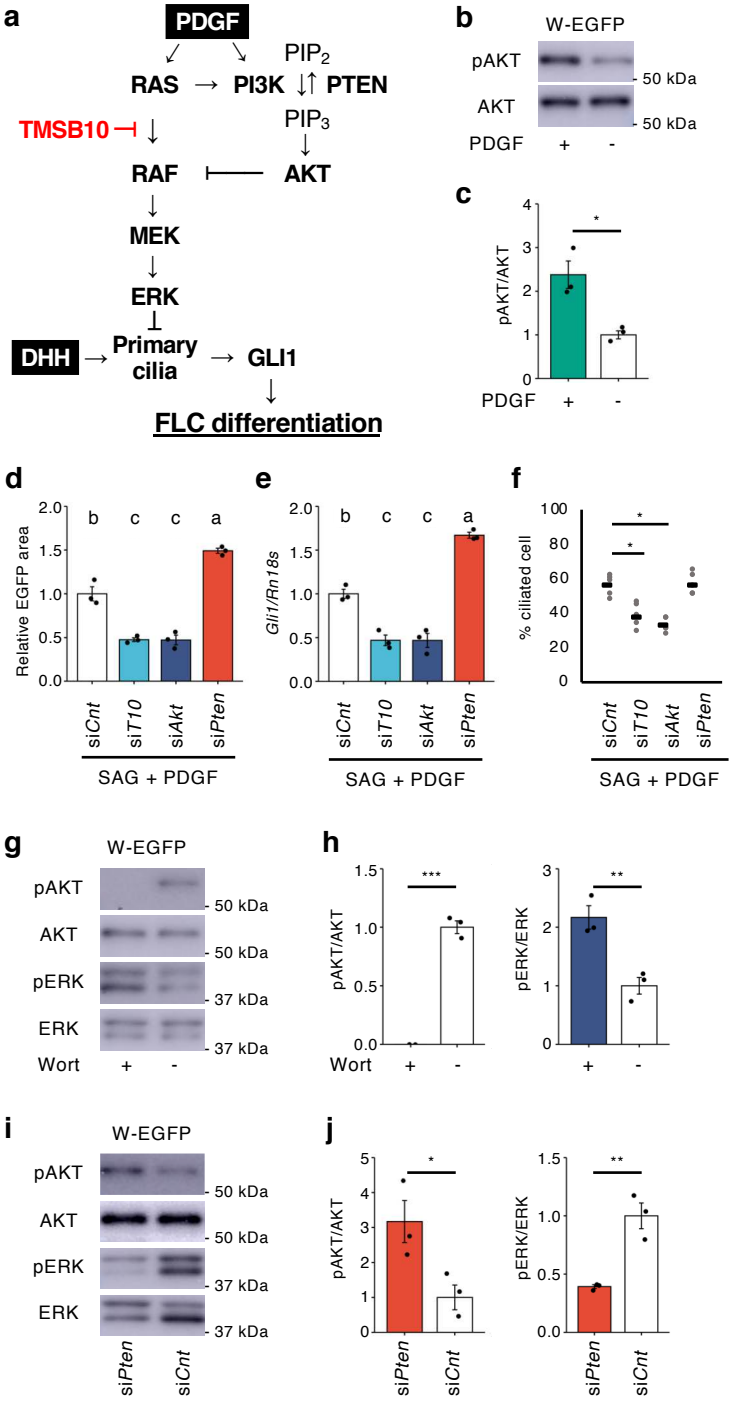
a
PDGF
PIP2
RAS → PI3K ↓↑ PTEN
TMSB10 ⊣
PIP3
RAF ⊣ AKT
MEK
ERK
DHH → Primary cilia → GLI1
FLC differentiation
b
W-EGFP
pAKT
AKT
50 kDa
50 kDa
PDGF + -
c
pAKT/AKT
PDGF + -
d
Relative EGFP area
b c c a
siCnt siT10 siAkt siPten
SAG + PDGF
e
Gli1/Rn18s
b c c a
siCnt siT10 siAkt siPten
SAG + PDGF
f
% ciliated cell
siCnt siT10 siAkt siPten
SAG + PDGF
g
W-EGFP
pAKT
AKT
pERK
ERK
50 kDa
50 kDa
37 kDa
37 kDa
Wort + -
h
pAKT/AKT
Wort + -
pERK/ERK
+ -
i
W-EGFP
pAKT
AKT
pERK
ERK
50 kDa
50 kDa
37 kDa
37 kDa
siPten siCnt
j
pAKT/AKT
siPten siCnt
pERK/ERK
siPten siCnt

Figure 6. Dual role of PDGF in regulating FLC differentiation

(a) A schematic summary of signal pathways regulating FLC differentiation and in which *Tmsb10* acts as a suppressor. ***(b)*** W-EGFP cells were cultured in the presence (+) or absence (-) of PDGF-AA. Whole-cell extracts prepared from the cells were subjected to Western blotting for phospho-AKT (pAKT) and AKT. Representative images of the blots are shown. The positions of molecular weight markers are indicated at the left. ***(c)*** Signal intensities in the blots above were quantified as described in the Materials and Methods. The amounts of pAKT relative to AKT are shown. $n = 3$. *$p<0.05$. ***(d)*** W-EGFP cells were treated with si*Cnt*, si*T10*, si*Akt*, or si*Pten*, and then used for testis reconstruction. The reconstructed testes were cultured in the presence of SAG and PDGF for 21 days. The EGFP-positive cells in the reconstructed testes were quantified. $n = 3$. $p<0.001$. ***(e)*** W-EGFP cells were cultured under the same conditions as above. Expression of *Gli1* in the cells was determined by qRT-PCR. The data were normalized by *Rn18s* and are presented as means ± SEM. $n = 3$. $p<0.001$. Letters a, b, and c on the bars in *(d)* and *(e)* denote significant differences. ***(f)*** W-EGFP cells were cultured under the same conditions as above. Ciliogenesis in the W-EGFP cells was examined by immunostaining for ARL13B. $n = 5$. *$p<0.001$. ***(g)*** W-EGFP cells were cultured in the presence (+) or absence (-) of wortmannin (Wort). Whole-cell extracts were subjected to Western blotting for pAKT, AKT, pERK, and ERK. ***(h)*** Signal intensities in the blots above were quantified as described in the Materials and Methods. The amounts of pAKT relative to AKT (left) and pERK relative to ERK (right) are shown. $n = 3$. **$p<0.01$. ***$p<0.001$. ***(i)*** W-EGFP cells treated with siRNA for si*Pten* and si*Cnt*. Whole-cell extracts prepared from the cells were subjected to Western blotting for pAKT, AKT, pERK, and ERK. Full blot images for *(b)*, *(g)*, and *(i)* are shown in Supplemental Fig. 8. ***(j)*** Signal intensities in the blots above were quantified. The amounts of pAKT relative to AKT (left) and pERK relative to ERK (right) are shown. $n = 3$. *$p<0.05$. **$p<0.01$.

Supplementary Files

This is a list of supplementary files associated with this preprint. Click to download.

- SupInfoTmsb102022220214.pdf